

Cosmic Web Dynamics: Forces and Strains

Roi Kugel,^{1,2} Rien van de Weygaert,¹

¹*Kapteyn Astronomical Institute, University of Groningen, PO Box 800, 9747 AD, Groningen, The Netherlands*

²*Leiden Observatory, Leiden University, PO Box 9513, NL-2300 RA Leiden, the Netherlands*

Accepted XXX. Received YYY; in original form ZZZ

ABSTRACT

This study concerns an inventory of the gravitational force and tidal field induced by filaments, walls, cluster nodes and voids on Megaparsec scales and how they assemble and shape the Cosmic Web. The study is based on a $N_{\text{part}} = 512^3$ Λ CDM dark matter only N-body simulation in a $(300h^{-1} \text{ Mpc})^3$ box at $z = 0$. We invoke the density field NEXUS+ multiscale morphological procedure to assign the appropriate morphological feature to each location. We then determine the contribution by each of the cosmic web components to the local gravitational and tidal forces. We find that filaments are, by far, the dominant dynamical component in the interior of filaments, in the majority of underdense void regions and in all wall regions. The gravitational influence of cluster nodes is limited, and they are only dominant in their immediate vicinity. The force field induced by voids is marked by divergent outflowing patterns, yielding the impression of a segmented volume in which voids push matter towards their boundaries. Voids manifest themselves strongly in the tidal field as a cellular tapestry that is closely linked to the multiscale cosmic web. However, even within the interior of voids, the dynamical influence of the surrounding filaments is stronger than the outward push by voids. Therefore, the dynamics of voids cannot be understood without taking into account the influence of the environment. We conclude that filaments constitute the overpowering gravitational agent of the cosmic web, while voids are responsible for the cosmic web’s spatial organisation and hence of its spatial connectivity.

Key words: large-scale structure of Universe – cosmology: theory – dark matter

1 INTRODUCTION

This study concerns a systematic inventory of the gravitational force and tidal field on Megaparsec scales and its role in determining the structure of the Cosmic Web. We assess the force field and tidal field induced by filaments, walls, cluster nodes and voids, and assess in how far they contribute, and dominate, the gravity and tides in the various regions of the cosmic web. It allows us to investigate the question which morphological features in the large scale universe dominate - and drive - the gravitationally driven formation and evolution of the largest structure in the universe. Also, as this will depend to a considerable extent on location, we include a systematic inventory of the identity of the regions over which voids, filaments and clusters dominate the the gravitational and tidal force. In an accompanying study, we specifically focus on the dynamical influence of cosmic voids in the large scale matter distribution, which represent the major share of the cosmic volume and who - along with filaments - dominate the dynamics of the large scale Universe.

1.1 The Cosmic Web: structure and detection

The *Cosmic Web* is the intricate multiscale network defined by the matter and galaxy distribution on Megaparsec scale (Zeldovich 1970; Einasto 1977; Bond et al. 1996; van de Weygaert & Bond 2008a; Cautun et al. 2014). It represents the fundamental spatial organisation of matter on scales of a few up to a hundred Megaparsec. Galaxies, intergalactic gas and dark matter arrange themselves in a salient wispy pattern of dense compact clusters, long elongated filaments,

and sheetlike tenuous walls surrounding near-empty void regions. Filaments are the most visually outstanding features of the Megaparsec Universe, in which around 50% of the mass and galaxies in the Universe resides. On the other hand, almost 80% of the cosmic volume belongs to the interior of voids (see e.g. Cautun et al. 2014; Ganeshaiiah Veena et al. 2018). Together, they define a complex spatial pattern of intricately connected structures, displaying a rich geometry with multiple morphologies and shapes. This complexity is considerably enhanced by its intrinsic multiscale nature, including objects over a considerable range of spatial scales and densities. The connectivity of this rich pallet of features, the nature of how the various structures connect to establish the pervasive network, has only recently been recognised as an important defining - topological - aspect (Aragón-Calvo et al. 2010; Shim et al. 2021; Wilding et al. 2021; Feldbrugge & van de Weygaert 2023). For a recent up-to-date report on a wide range of relevant aspects of the cosmic web, we refer to the volume by van de Weygaert et al. (2014).

In the observational reality, the existence and structure of the Cosmic Web has been revealed in the most detail by maps of the nearby cosmos produced by large galaxy redshift surveys. Starting from first revelation of the web-like arrangement of galaxies by the CfA2 survey (e.g. de Lapparent et al. 1986), subsequent surveys such as 2dFGRS, the SDSS, the 2MASS and GAMA redshift surveys (Colless et al. 2003; Tegmark et al. 2004; Huchra et al. 2012; Liske et al. 2015) established the web-like arrangement of galaxies as a fundamental characteristic of cosmic structure. Maps of the galaxy distribution at larger cosmic depths, such as VIPERS (de la Torre et al. 2013), showed its existence over a sizeable fraction of cosmic time.

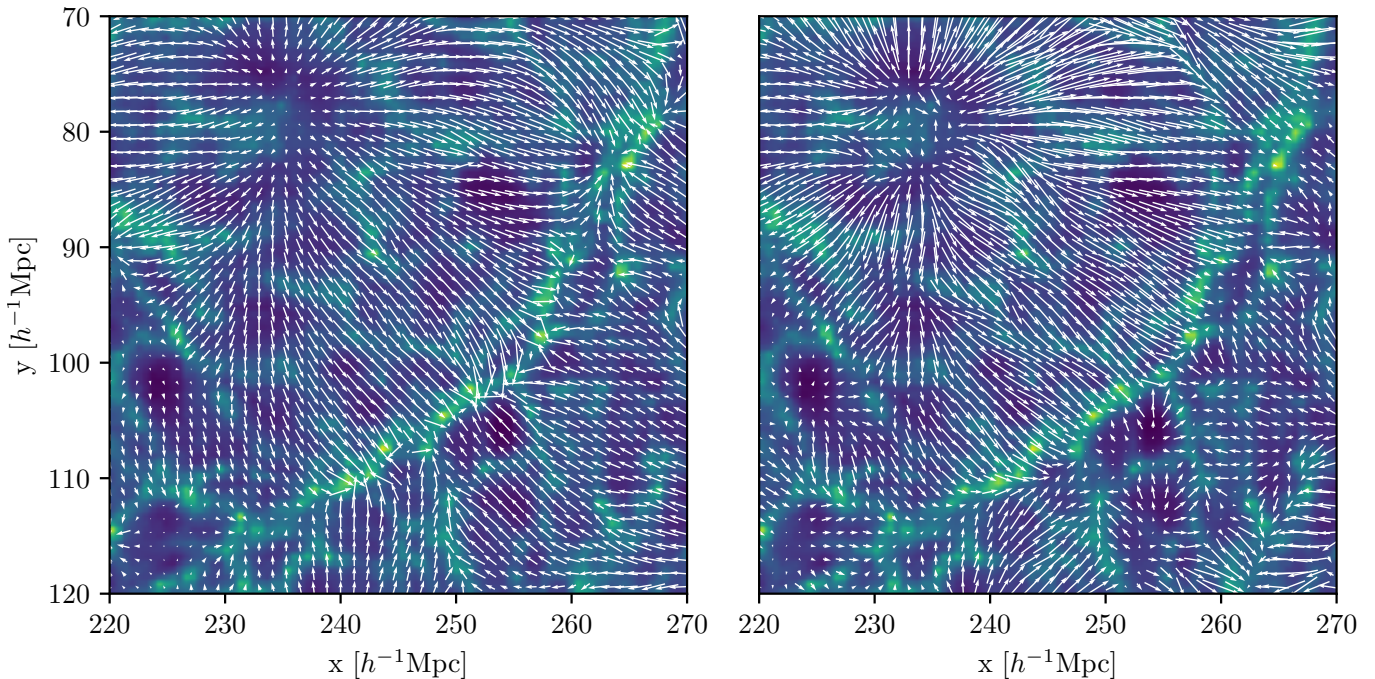


Figure 1. Gravitational force field in and near a void. Left: the force vectors representing the local direction and amplitude of the total gravitational force, i.e. the force exerted by the total cosmic mass distribution. Right: the local force vectors resulting from the combined influence of mass elements in void regions. The vector lengths are normalised with respect to the local total velocity and show the relative contribution of the field at that location.

Also the intergalactic gaseous medium, closely follows the web-like structure defined by the dark matter, the principal component of the cosmic web. A range of observational probes have detected the web-like structure over which intergalactic gas, in a range of thermodynamic states (see [Meiksin 2009](#), for a review), has diffused itself. Ly α absorption lines in the spectra of bright background sources such as QSOs are piercing through the web-like assembly of neutral hydrogen gas in the cosmic web at high redshifts ([Ostriker & Cen 1996](#); [Cen 1997](#)). The combination of sufficiently close linear probes even allows a reconstruction of the full three-dimensional intergalactic hydrogen lanes ([Pichon & Bernardeau 1999](#)).

It has already led the Clamato survey ([Lee et al. 2018](#)) to successfully produce fascinating maps of the full three-dimensional gaseous cosmic web at high redshifts. Recent observations by the MUSE integral field unit on the very large telescope, even managed to see the Ly α emission from the filamentary gaseous extensions around clusters directly. At lower redshifts, most of the intergalactic gas has heated up as it settled in the deepening potential wells of the dark matter cosmic web. This warm gas, the so called WHIM, is assumed to represent the major share of baryons in the current Universe. As such is a prime target for detection and mapping ([Nicastro et al. 2018](#); [Macquart et al. 2020](#)), although it had proven to be notoriously hard to detect. It has been more straightforward to detect the hot gas residing in the strongest filamentary features in the cosmic web at high redshifts, filling the short dense bridges between two adjacent clusters. The hot gas reveals itself through the Sunyaev-Zeldovich upscattering of CMB photons. It has even allowed the detection of a few individual high-redshift gaseous filaments, where their ubiquitous presence has been revealed by stacking numerous cluster pair Sunyaev-Zeldovich observations ([Bonjean et al. 2018](#); [de Graaff et al. 2019](#)).

1.2 The Cosmic Web: dynamics, formation and evolution

The origin of the cosmic web is to be found in the tiny inhomogeneities in the primordial spatial matter distribution. These induce an inhomogeneous and anisotropic gravitational force field. It sets off the migration of matter, culminating in the continuous growth of density and velocity inhomogeneities ([Peebles 1980](#)). Ultimately, as the matter fluctuations become nonlinear, it leads to the contraction and collapse of structures and expansion of underdense regions. At the transition from the initial long phase of linear growth of the primordial (Gaussian) density field and density field to the complex structured nonlinear mass distribution, we find the emergence of the intriguing and complex spatial pattern of the *Cosmic Web*. It marks the cosmic web as a key phase in the dynamical buildup of structure in the Universe.

A plethora of cosmological computer simulations ([White et al. 1987](#); [Springel 2005](#); [Pillepich et al. 2018](#); [Bocquet et al. 2020](#); [Angulo et al. 2021](#)), including more elaborate cosmological hydrodynamics simulations (e.g. [Hirschmann et al. 2014](#); [Schaye et al. 2015](#); [McCarthy et al. 2017](#); [Pillepich et al. 2018](#); [Schaye et al. 2023](#)) revealed that through gravitationally driven evolution the Gaussian initial density and velocity perturbations morph into an intricate web-like pattern that resembles that seen in the spatial distribution of galaxies. The simulations show that the cosmic web is a fundamental aspect of structure formation in the standard Λ CDM cosmology, although this also turns out to be true for variations around the standard Λ CDM model (for a review see [Frieman et al. 2008](#)).

Within the context of the gravitational buildup of the cosmic web, the gravitational forces induced by the inhomogeneous mass distribution are the agent for the buildup of structure. They are instrumental in directing the cosmic migration streams that transport matter from low density areas to emerging matter concentrations. The accompanying tidal force field is the key towards shaping the mass distribution into

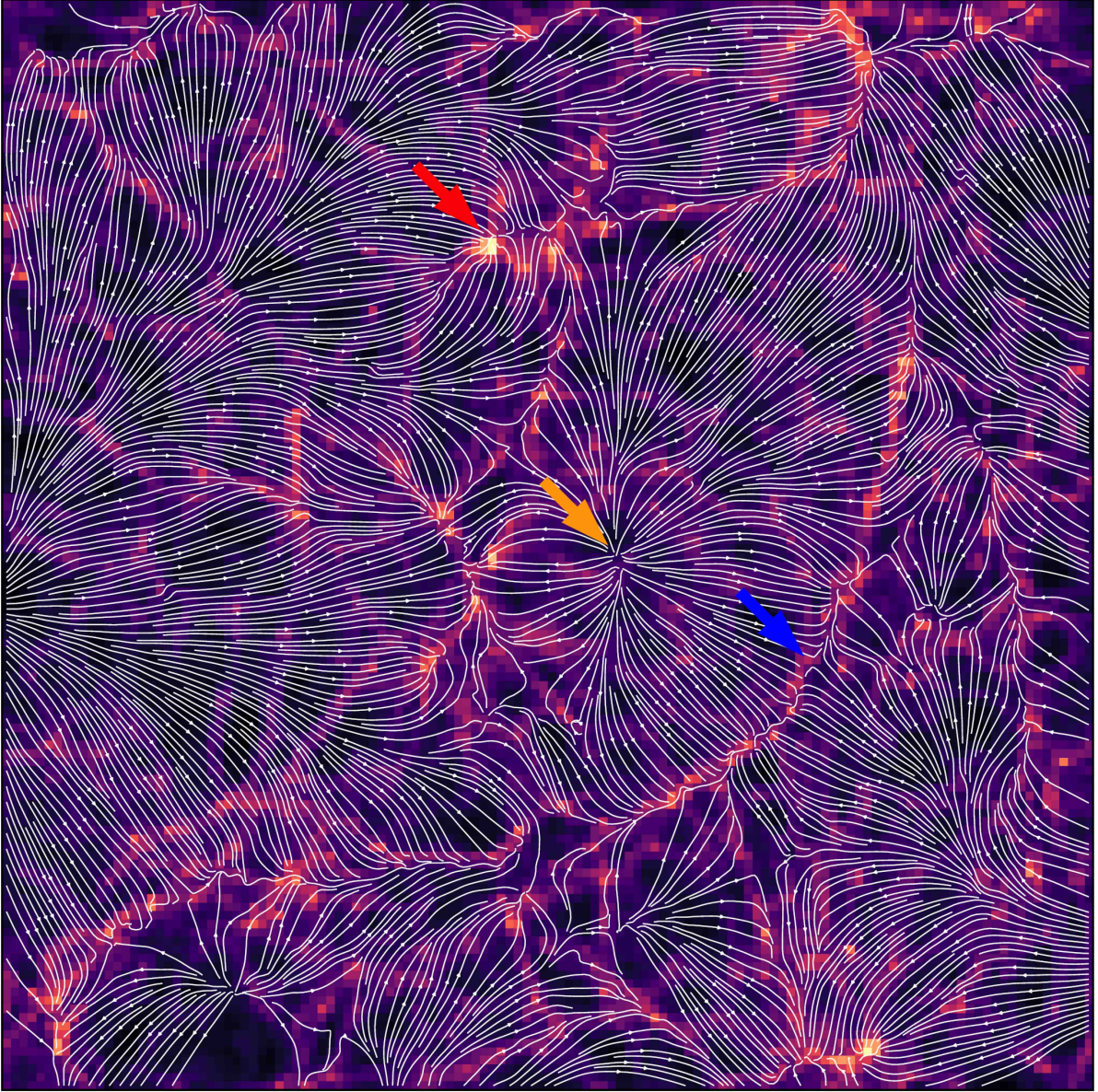


Figure 2. Flows of matter in the cosmic web. Superimposed on the (logarithmic) map of the cosmic density field in a slice of the simulation box are the streamlines of the corresponding cosmic velocity field. Arrows indicate three different aspects of the flow field: The red arrow highlights velocity inflow into a cluster node (negative divergence), the orange arrow highlights velocity outflow from a void (positive divergence) and the blue arrow highlights shear flow along a filament.

a weblike pattern. This had already been recognized and accurately described in the mildly nonlinear stage by the Zel'dovich formalism (Zeldovich 1970; Shandarin & Zeldovich 1989). The formation and evolution of the characteristic anisotropic structures, i.e. the filaments and walls, are the product of the anisotropic tidal strains and resulting anisotropic flow field and deformations (Bond et al. 1996; Hahn et al. 2007; van de Weygaert & Bond 2008a; Lee et al. 2009; Lee & Springel 2010; Hahn et al. 2010; Wang et al. 2014; Feldbrugge et al. 2018a; Feldbrugge & van de Weygaert 2024). It establishes a close relation between the weblike structures and the anisotropy of the induced migration flows, which has been the focus of a few insightful studies (Kitaura et al. 2012a; Hoffman et al. 2012; Wang et al. 2014). Recent work has also revealed the extent to which the spatial structure of the tidal force field determines the connections

between the components of the cosmic web. The connectivity can even already be recognised in the primordial tidal and deformation field, showing the extent towards which the primordial anisotropic force field is steering and shaping the structure of the emerging cosmic web (see eg. Wilding 2022; Feldbrugge et al. 2023; Feldbrugge & van de Weygaert 2024). It even leads to the realization that embryonic outline of the cosmic web, in particular its filamentary network, can already be seen in the primordial tidal eigenvalue field (Wilding 2022; Feldbrugge et al. 2023) (see figure 3).

For insight into the nature and origin of the characteristic properties of the cosmic web and for identifying the dependence of these on cosmology and cosmological parameters, theoretical understanding of the physical mechanisms and processes behind the emergence of the cosmic web. Analytical approximation and model have been es-

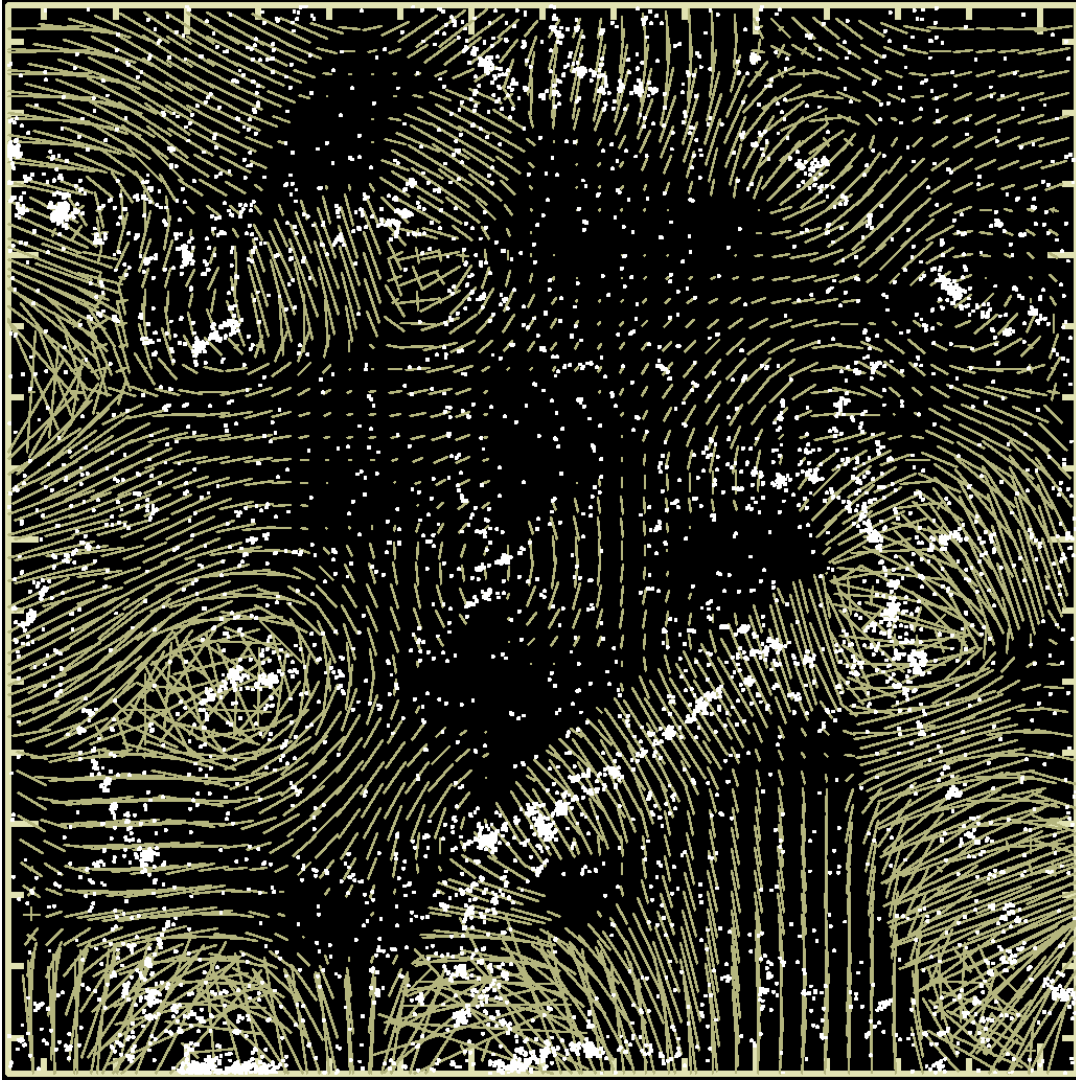


Figure 3. Cosmic web and tidal force field: the relation between the cosmic web and the spatial pattern of the corresponding compressional tidal field components. The image shows an LCDM matter distribution at the present cosmic epoch, along with the (compressional component) tidal bars in a $5h^{-1}$ Mpc thin central slice. The simulation is a realization of a dark matter only CDM based scenario (in an open, $\Omega = 0.3$ Universe. The tides are determined on a scale $R_G = 2h^{-1}$ Mpc). The matter distribution, displaying a pronounced weblike geometry, is clearly intimately linked with the characteristic coherent compressional tidal bar pattern.

sential in interpreting the results of surveys, as well as of simulations (e.g. Zeldovich 1970; Hidding et al. 2012; Wang et al. 2014; Hidding et al. 2016; Feldbrugge et al. 2018a; Feldbrugge & van de Weygaert 2024). An important aspect of the formation process are the forces and strains that shaped cosmic structure. For example, the phase-space based *Caustic Skeleton* model by Feldbrugge et al. (2018a) demonstrated that a full understanding of the cosmic web structure is obtained through the spatial characteristics of the *eigenvalue* and *eigenvector* fields of the cosmic tidal force field. Motivated by these considerations, the intention of the present investigation and inventory of the dynamics of the cosmic web is to establish the role of the various morphological features of the cosmic web in its formation and dynamical evolution. It involves the assessment of in how far the various elements of the cosmic web are formed and have evolved, and how they connect up in the complex, intricate pervasive network of the cosmic web.

While many structural aspects of the cosmic web have been addressed by numerous studies, its dynamics and dynamical evolution

has only been - superficially - explored within a purely theoretical or simulation context. Over recent years, we have seen that the dynamics behind the formation and evolution of the cosmic web is becoming increasingly accessible to observational investigation (see eg. Kitauro et al. 2012b). The forces and tides that shape the complex spatial pattern induce nonlinear migration currents, marked by distinct divergent and shear-like flows, have recently been traced in new, densely probed, galaxy peculiar velocity surveys. The most notable examples of this are the Cosmicflows-3 and Cosmicflows-4 (Tully et al. 2016; Kourkchi et al. 2020) surveys, a view that will be considerably extended by DESI (Schlafly et al. 2023). Including the peculiar velocity information even allowed to identify the impact of some individual components of the cosmic web is also found in the local universe. This concerns in particular the gravitational influence of voids: Tully et al. (2008) concluded that the Local Void has a large contribution of no less than $\sim 240\text{km/s}$ to the peculiar velocity of the Local Group.

Also the subtle morphing influence of the tidal forces has become

susceptible to observational scrutiny. The distinct anisotropic shape of the filaments and walls in the cosmic web is the direct outcome of the gravitationally driven formation of the cosmic web by the large scale anisotropic force field (van de Weygaert & Bond 2008a). Even the population of voids on Megaparsec scales is noticeably shaped and aligned by the large scale tidal force field (Park & Lee 2007; Platen et al. 2008).

Arguably the most prominent manifestation of the (tidal) anisotropic force field induced by the inhomogeneous matter distribution in the Universe is that of gravitational lensing. Hence, at a global level the tidal dynamics of the cosmic web is reflected in the corresponding deformation of galaxy images. In case the distortions are linear, inversion allows the study of the generating (projected) mass distribution. At present, gravitational lensing has become one of the most powerful probes of the global Universe and the cosmological parameters characterising it. With the availability of the upcoming powerful and accurate cosmological surveys, such as enabled by the Vera Rubin observatory and Euclid, the tedious lensing studies may even resolve the web-like nature of dark matter distribution. A few gravitational lensing studies have even already managed to detect and resolve filamentary dark matter bridges between nearby massive clusters (Dietrich et al. 2012). Amongst the most massive representatives amongst the filament population (Cautun et al. 2014), they leave a rather accessible and detectable lensing imprint.

Also at galaxy scales, the large scale tidal forces induce noticeable signatures (see e.g. van de Weygaert & Babul 1994; Paranjape 2021; Alam et al. 2024). Perhaps the most outstanding manifestation is that of the alignment of the spin axis of collapsing dark matter halos with the filaments in which they are embedded, and hence that of the corresponding rotation axis of galaxies. It is clear from observations (see Jones et al. 2010; Tempel et al. 2013; Welker et al. 2020) that the rotation axis of galaxies preferentially align with the components of the cosmic web. Largely the result of the imparted tidal torques on the collapsing halos (Hoyle 1949; Peebles 1969; Efstathiou & Jones 1980; White 1984; Lee & Pen 2000; Porciani et al. 2002a,b; Schäfer 2009), additional secondary effects responsible for the mass dependence of the spin orientation (Aragón-Calvo et al. 2010; Hahn et al. 2007, 2010; Codis et al. 2012; Tempel et al. 2013; Ganeshaiiah Veena et al. 2018, 2019; López et al. 2021; Zhang et al. 2023) may be the result of the induced filamentary inflow of mass (Ganeshaiiah Veena et al. 2021). The latter has become a key issue of attention, given the implications for gravitational lensing studies.

1.3 Morphology of the Cosmic Web

While the cosmic web has four morphologically well defined features, there are many ways to identify the different components. Over the past decades, a range of methods and formalisms have been put forward for the detection and classification of filaments. A review and comparison of more than a dozen formalisms can be found in Libeskind et al. (2018). They distinguish at least five classes of formalisms to classify and analyse the cosmic web. Geometric filament finders are usually based on the Hessian of the density or gravitational potential at each location. It includes the Tweb and Vweb formalisms (Hahn et al. 2007; Forero-Romero et al. 2009; Hoffman et al. 2012), which emphasize and exploit the intimate link between the tidal force field and induced anisotropic velocity flows and the spatial structure and connectivity of the weblike pattern that is emanating as a result of these. The most sophisticated ones explicitly take into account the multiscale nature of the mass distribution, of which MMF/Nexus is a particular example (Aragón-Calvo et al. 2010; Cautun et al. 2013). Topological methods address the connections between structural sin-

gularities in the mass distribution. They are amongst the most widely used formalisms in the studies of the cosmic web, in particular, that of Disperse (Sousbie 2011; Sousbie et al. 2011). Other representatives are Spineweb (Aragón-Calvo et al. 2007a) and Felix (Shivashankar et al. 2016).

In addition to the geometric and topological formalisms, several alternative methods have played a substantial role in the study of the cosmic web. Bisous is a well-known stochastic formalism, involving Bayesian exploration based on stochastic geometric modelling of filaments (Tempel et al. 2014a). It forms the basis for the widely used filament catalogue extracted from the SDSS survey (Tempel et al. 2014b). More recent developments often incorporate machine learning codes (see e.g. Awad et al. 2023). Perhaps the oldest representatives for a systematic analysis of filamentary patterns are graph-based methods. The Minimal Spanning Tree (MST) is a prime example and is figuring prominently in the cosmic web analysis of the GAMA survey (Alpaslan et al. 2014). There is even a class of cosmic web identifiers that exploit the resemblance of the cosmic web to biological branching networks. The Monte Carlo Physarum Machine, inspired by the growth of Physarum polycephalum 'slime mold', has been successfully applied to the structural analysis of the cosmic web in both simulations and observations (Elek et al. 2020, 2022; Wilde et al. 2023).

Possibly the most profound techniques for classification of the cosmic web are those emanating from the analysis of the 6D phase-space structure of the cosmic mass distribution (Shandarin 2011; Shandarin et al. 2012; Neyrinck & Shandarin 2012; Abel et al. 2012). Restricted to situations in which the initial conditions are known, they yield the identification of the matter streams constituting the migration of mass in the buildup of structure. It allows the definition of an objective physical criterion for what constitutes the various structural elements of the cosmic web. The recent study by Feldbrugge & van de Weygaert (2024) on the phase-space based dynamical specification of the nature of cosmic filaments emanates from a detailed phase-space based assessment of cosmic structure formation, within the context of the Caustic Skeleton model for the formation of the cosmic web (Feldbrugge et al. 2018b).

The present study is based on the MMF/Nexus morphology classification formalism (Aragón-Calvo et al. 2007b,a, 2010; Cautun et al. 2013, 2014), that is unique in addressing both the geometric nature as well as the multiscale nature of the cosmic matter distribution. By means of the Hessian of the density field NEXUS to find the geometric/morphological signature of the individual components. Of particular interest for our purpose is the NEXUS+ flavour of NEXUS. It applies log-space filtering to the density field before identification. Like shown by Cautun et al. (2014) this allows NEXUS+ to find even the more tenuous elements of the cosmic web.

1.4 Cosmic Web Dynamical Inventory

The present study extends the previous cosmic web inventory of Cautun et al. (2014) to that of the corresponding force and tidal field influence as a function of cosmic web environment. The distinct structure of the morphological elements of the cosmic web implies that each component will also be dynamically distinct, both in its local dynamics, but also in the influence it will have on its surroundings through the force and tidal field. Bond et al. (1996) argue that the main origin of filaments in the cosmic web is due to the distribution of nodes in the cosmic web, and not much work has been done on the topic since. In this work we aim to extend our knowledge about the dynamical influence and origin of the cosmic web.

To quantify the dynamical influence, we analyse a Λ CDM (dark

matter only) simulation, and asses at each location in a cosmic volume the contribution by filaments, walls, voids and nodes to the local gravitational and tidal force (see eg. fig. 1 for the force field contribution by voids). This allows a statistical inventory of the dynamical dominance of the various morphological elements of the cosmic web. To this end we apply NEXUS+ to identify for each point in the simulation whether it belongs to a filaments, wall, void or node. Using direct summation over the gridcells, we are then able to construct the force and tidal field originating from each component.

The obtained fields are full vector fields, for the force field, or matrix fields, for the tidal field. This allows us to study both the morphology and the strength of the fields belonging to each component. For each field we look at both the (relative) amplitude and the direction. In addition, the spatial coherence and pattern of the induced flow field is studied on the basis of streamline maps (see fig. 2). We are also able to zoom in on a few specific regions to study the interplay between the different components. In this way we are able to find where, and how the different components contribute to the total force field. By looking at the tidal field we are also able to assess which component is responsible for creating the an-isotropic nature of the cosmic web (see fig. 3).

1.5 Outline

This paper is structured as follows. In section 2 we describe the simulation we use, how we obtain the identification of the cosmic web components and how we calculate the force and tidal fields. In section 4 we describe the force field of the individual components for the complete $(300\text{Mpc})^2$ slice. In section 5 we investigate two smaller regions of the full slice, and look at the force fields around a void and a node. In section 6 we describe our results for the tidal field. We finish by summarising our conclusions in section 8.

2 DATA AND ANALYSIS: N-BODY SIMULATIONS

For the dynamical inventory of the cosmic web in the present study, we analyze a LCDM dark matter only cosmological N-body simulation. The force and tidal inventory in the present study largely pertains to the current cosmic epoch, redshift $z = 0$. The evolution of the force and tidal force fields will be analyzed in an accompanying upcoming publication. In this section we describe the specific methods and formalisms used to get to the inventory of the gravitational force and tidal field within this simulation.

The simulation is processed and analyzed with a set of instruments that allow the optimal identification of the multiscale structure and dynamics of the cosmic web. These include the translation from the discrete set of particle position and velocities towards continuous density and flow fields that optimally retains the anisotropic pattern of the cosmic web as well as its multiscale structure. This is accomplished through the use of the DTFE formalism (Schaap & van de Weygaert 2000; van de Weygaert & Schaap 2009; Cautun & van de Weygaert 2011).

Instrumental in our study is the classification and identification of the morphological components of the cosmic web. The morphological identification and classification of the geometric components of the cosmic web is based on the use of the MMF/Nexus formalism, specifically that of NEXUS+ version of the MMF/Nexus pipeline (Aragón-Calvo et al. 2007a; Cautun et al. 2013).

The second major aspect of our analysis concerns the calculation of the (peculiar) gravity and tidal fields, globally as well specific for those induced by the individual components of the cosmic web. The

computational details are described in section 3.1. To appreciate the spatial structure of the force and tidal fields better, and to interpret the results obtained, in section 3.1.1 we include a description of the various aspects of visualisation of these fields.

The necessary details of the Nbody simulation and applied analysis tools are outlined below.

2.1 N-body Simulation

The study is based on the analysis of the N-body, dark matter only simulation described in Bos (2016). The cosmological context is that of a Λ CDM cosmology with WMAP 3-year parameter values: $\Omega_m = 0.268$, $\Omega_\Lambda = 0.732$, $\Omega_{bZel} = 0.044$, $h = 0.704$, $\sigma_8 = 0.776$ and $n = 0.947$. The simulation contains 512^3 dark matter particles in a simulation box with a boxlength of $300 h^{-1}$ Mpc. The simulations start at $z = 60$, following the initial displacement and velocity set by the Zeldovich approximation (Zeldovich 1970). The analysis described in the present study focuses on the on the inventory of the force and tidal field at the current epoch, $z = 0$.

2.2 DTFE Density and Velocity maps

To translate the spatial particle distribution into density and velocity maps, we convert the particle locations and velocities into a space-filling DTFE density and velocity maps. The density Δ ,

$$\Delta = \frac{\rho}{\rho_u} = \delta + 1 \quad (1)$$

and velocity field \mathbf{v}_{DTFE} are sampled on a 512^3 grid. It corresponds to a resolution of $0.59 h^{-1}$ Mpc for each grid cell.

The Delaunay tessellation field estimator (DTFE) (Schaap & van de Weygaert 2000; van de Weygaert & Schaap 2009; Cautun et al. 2013), uses the Voronoi and Delaunay tessellation of the spatial particle distribution to get an unbiased volume-weighted estimate of the local density including a natural interpolation over the entire volume using the dual Delaunay tessellation as natural interpolation grid. Application of DTFE to the velocity field, traced by the simulation particles, not only yields a volume-weighted space covering reconstruction of the velocity field but also yields maps of the first order gradient of the flow field, ie. the divergence and shear (and even vorticity) of the flow field (Bernardeau et al. 1997; van de Weygaert & Bernardeau 1998; Romano-Díaz & van de Weygaert 2007; van de Weygaert & Schaap 2009). THE DTFE density and velocity fields are sampled on a 512^3 grid.

2.3 MMF/NEXUS+

To dissect the cosmic matter distribution into the various morphological components of the cosmic web we use the MMF/NEXUS pipeline, specifically its NEXUS+ version (Cautun et al. 2013, 2014). It is the highest dynamic range version of the NEXUS library of routines for pattern classification based on the MMF/Nexus Multiscale Morphology Filter formalism (Aragón-Calvo et al. 2007a,b, 2010; Cautun et al. 2013, 2014). For a short review see appendix A, as well as Libeskind et al. (2018). We specifically chose to use the NEXUS+ version as it is optimally suited to take into account the multiscale nature and the wide dynamic range of cosmic web density field (Cautun et al. 2014). Compared with the other NEXUS methods it provides the sharpest rendering of the cosmic web, including the more tenuous walls and filaments.

Instrumental and unique for the class of MMF cosmic web identification methods is that it simultaneously pays heed to two principal

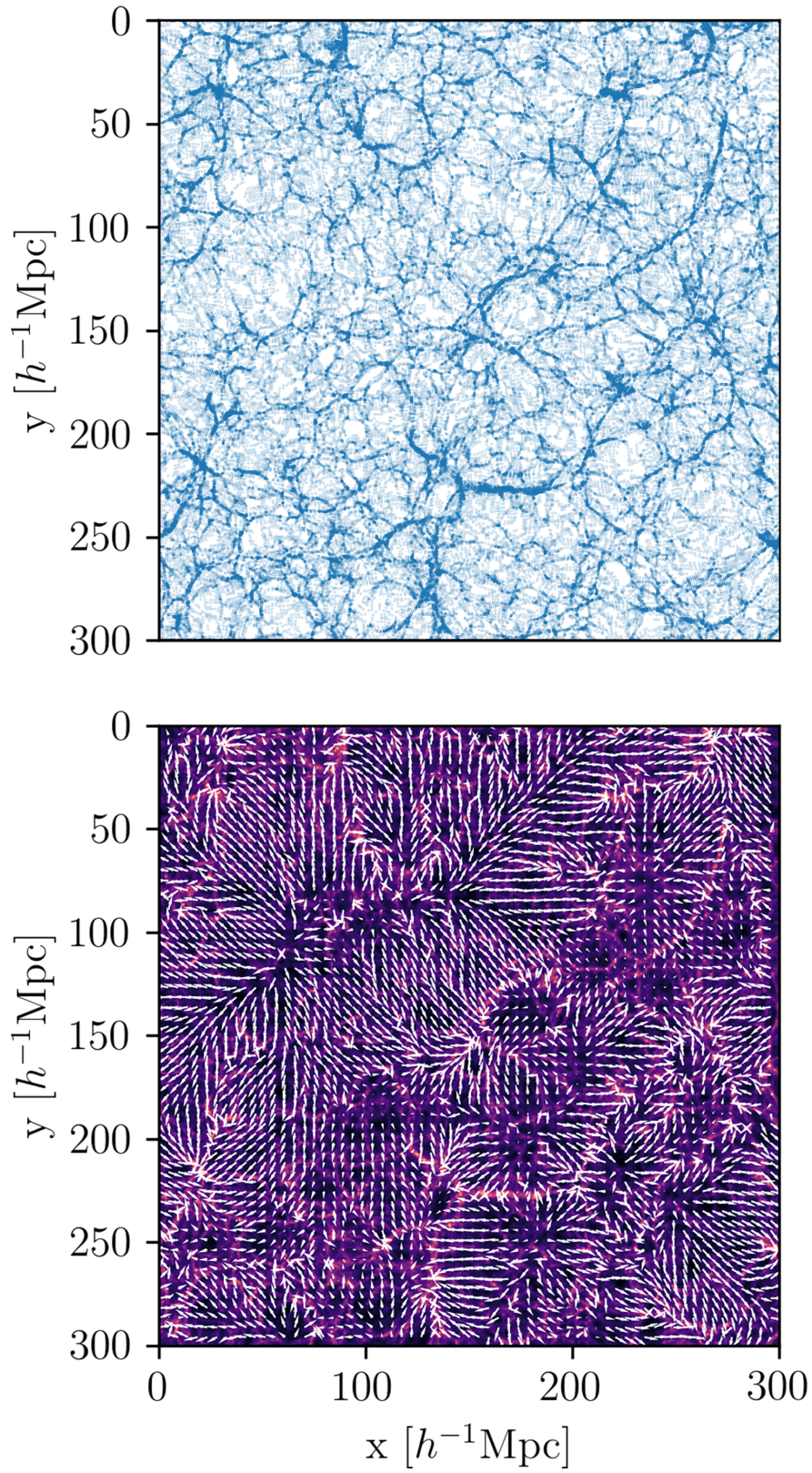


Figure 4. Cosmic Mass distribution and force field. Top panel: the particle distribution, at $z = 0$ in a $0.59 h^{-1}$ Mpc thick slice from a LCDM N-body simulation in a $300 h^{-1}$ Mpc by $300 h^{-1}$ Mpc box. Bottom panel: the corresponding gravity force vector plot in the same slice.

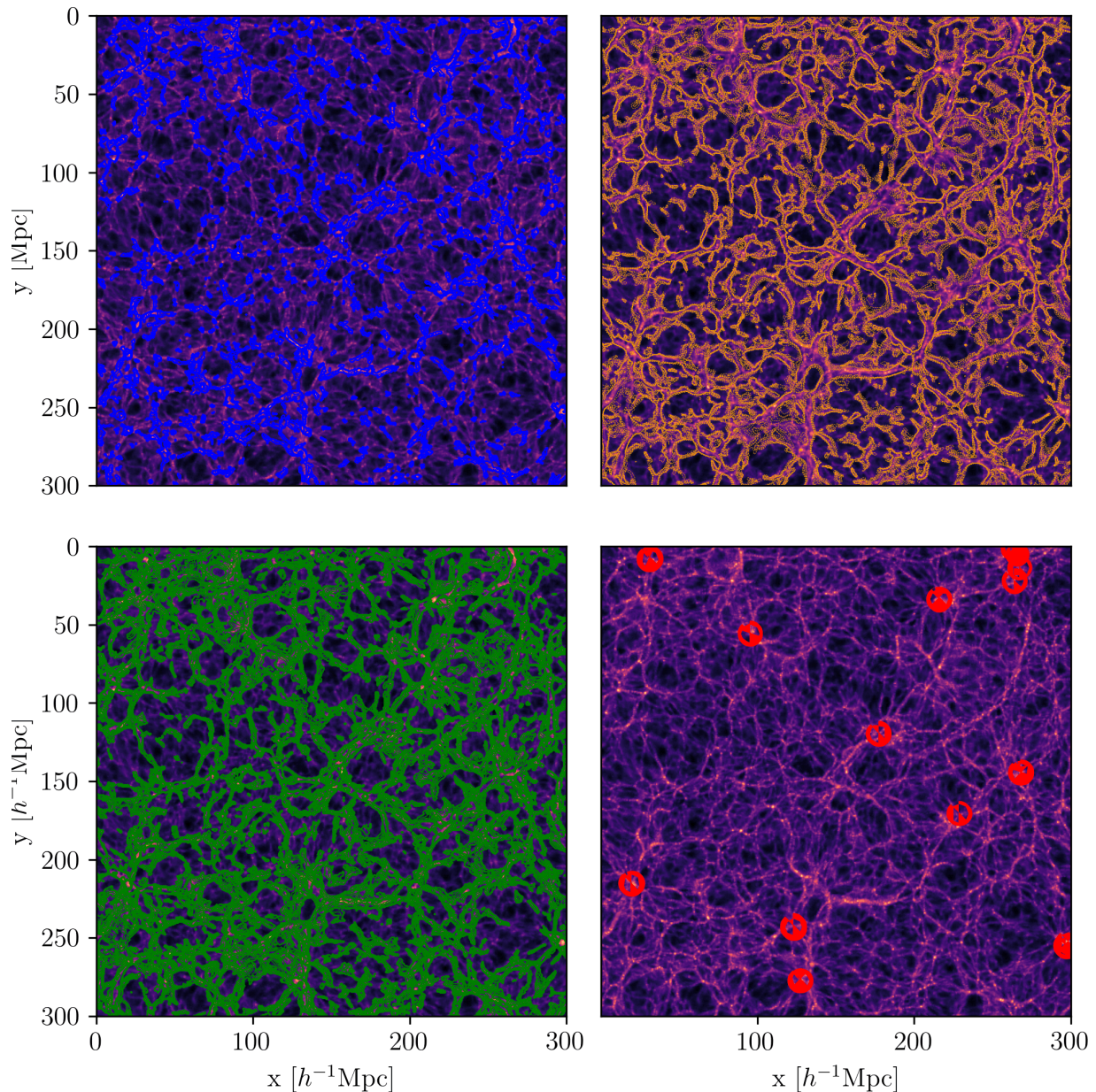


Figure 5. Cosmic web components identified by Nexus+: filaments, voids, walls and cluster nodes. Each panel shows a representation of a $300 h^{-1}\text{Mpc}$ by $300 h^{-1}\text{Mpc}$ by $0.59 h^{-1}\text{Mpc}$ slice from the N-body simulation used. Top left panel: Filaments. The NEXUS+ filament contours, in blue, are superimposed on the log density field. Top right panel: Voids. The NEXUS+ void boundary contours, in orange, are superimposed on the log density field. Bottom left panel: Walls. The NEXUS+ wall contours, in green, are superimposed on the log density field. Bottom right panel: Cluster nodes. The cluster nodes, indicated by red symbols, are superimposed on the log density field.

aspects characterising the web-like cosmic mass distribution. The first aspect is that of the different geometric shapes of the various structural components of the cosmic web, in particular the anisotropic shapes of filaments and walls. The Hessian of the corresponding fields translates into the local geometry and local anisotropy on the basis of the ratios of its eigenvalues. That is, it determines whether the mass distribution has a roundish, flattened or elongated geometry. The second aspect is that of the multiscale character of the cosmic mass distribution, the product of the hierarchical evolution and buildup of structure in the Universe. To this end, MMF/Nexus invokes a *Scale-Space* analysis to enable it to probe the scale dependence of the local geometry of the mass (or velocity or gravity) distribution. It allows the detection, and complete and unbiased characterisation, of

features present at all scales, from the prominent structures present in overdense regions to the tenuous networks pervading the cosmic voids.

The MMF/Nexus formalism results in a scale adaptive framework that classifies the matter distribution on the basis of local spatial variations in either the density field, velocity field or gravity field. Their geometry and anisotropy are encoded in the Hessian matrix determined at each of the spatial scales at which the fields are assessed. Subsequently, a set of morphological filters is used to classify the spatial matter distribution into three basic components, the clusters, filaments and walls that constitute the cosmic web. It produces a map in which for each location in the analysed volume the morphological identity is specified. The end product of the pipeline is a multiscale

Table 1. Mass and volume fractions of the different components of the cosmic web as identified by NEXUS+.

Component	Mass fraction [%]	Volume fraction [%]
Filaments	46.2	7.25
Voids	21.4	72.09
Nodes	4.6	20.65
Walls	27.8	0.01

identification of the cosmic web into its structural components. To this end, each location and mass element of the matter distribution is assigned a unique morphological identity as either belonging to a filament, cluster node, wall or void.

For more details on the MMF/Nexus formalism we refer to appendix A.

2.3.1 NEXUS+: practical implementation

While in principle the NEXUS *Scale Space* formalism involves an infinite number of scales, in our practical implementation we use a finite number of filter scales, restricted to the range of $[1.0, 4.0]h^{-1}\text{Mpc}$. We tested a few other filter ranges, and concluded that the used range provides a robust population of filaments. This includes the major dynamically dominant filaments, along with a fair fraction of the tenuous tendrils. We also assessed this for the higher redshift simulation snapshots, to find that for $z > 3.8$ most filaments are to be found in this scale range.

The morphological signature is evaluated on a 512^3 grid, ie. for each of the gridpoints on this grid NEXUS+ provides us with the identity of the morphological features to which it belongs.

3 FORCE AND STRAIN FIELD: PROCEDURE

For the computation of the diverse gravitational force and tidal fields, we use a brute force approach. At each grid location we compute the contributions by the various morphological elements of the cosmic web by summing the gravitational and tidal force contributions from the grid points located in the regions that have been identified with this morphology. In short, the force and tidal influence of filaments is the sum of the mass elements residing in filaments, of voids the sum of mass elements residing in voids, etc. The total (peculiar) gravitational force and tidal strain at each location is the sum of the contributions by all mass elements in the volume.

The stated force and tidal force calculations involve the following practical issues:

1. The gravitational force field and tidal strain field are evaluated on the same 512^3 grid as the one on which we have computed the DTFE density field, and assessed the NEXUS+ identity (see previous section).
2. The forces and tidal strains are computed by brute force, i.e. we compute these at a given location by summing the force and tidal contribution.
3. Following a sheer brute force summation, our computational resources allow us to carry out the computation for a restricted number of locations, instead of for all 512^3 gridpoints.
4. For the brute force computation, we assume that a spherical surrounding volume of radius $150h^{-1}\text{Mpc}$, corresponding to the largest sphere that fits inside the simulation box, is sufficient to include

all gravitationally relevant influences. In other words, force and tide contributions are considered to be negligible beyond a distance of $r = 150h^{-1}\text{Mpc}$. This is certainly true for the tidal contributions, and turns out to be valid to very good approximation for the gravitational force itself.

5. A more efficient Fourier space based formalism is under development, but has not yet been applied to the analysis of the simulation in this study. A Fourier code would automatically guarantee periodic boundary conditions pertaining to the simulation box, and hence by implication include the force and tidal influences throughout the entire simulation volume.

Because the brute force calculations are computationally intensive, we restricted the force and tidal evaluations to a few slices of the simulation box, yielding a total of 512^2 force evaluations on the corresponding 512^2 grid. The force at each point is computed using the full three dimensional grid, yielding a fully three dimensional force and tidal tensor at each gridpoint. For the statistical results presented in our study, we established that the force and tides on a 512^2 two-dimensional grid is representative and hence sufficient for our discussion. Figure 4 shows the resulting total force field. Figure 5 shows the NEXUS+ morphological identifications in the same slice. The volume and mass fractions for the different components of the cosmic web are given in Table 1.

3.1 Gravitational Force field

The peculiar gravitational force field for a continuous matter distribution field, specified in terms of the density perturbations $\delta_m(\mathbf{x})$,

$$\Delta_m(\mathbf{x}) = \frac{\rho(\mathbf{x}, t) - \rho_u(t)}{\rho_u(t)}, \quad (2)$$

The resulting peculiar gravity field, following Peebles (1980), is given by

$$\mathbf{g}(\mathbf{x}) = \frac{3\Omega_m H_0^2}{8\pi} \int d\mathbf{x}' \Delta_m(\mathbf{x}') \frac{\mathbf{x}' - \mathbf{x}}{|\mathbf{x}' - \mathbf{x}|^3}. \quad (3)$$

As we represent this field on a discrete grid, the force integral expression is converted into a sum over the mass-weighted contribution to the gravitational force by each gridpoint. Evaluating the force field at the gridpoint i , at location \mathbf{x}_i , the corresponding grid expression for the full force field $\mathbf{g}_i(\mathbf{x}_i)$ is the sum over all N gridpoints j , at locations \mathbf{x}'_j ,

$$\mathbf{g}_i(\mathbf{x}_i) = \frac{3\Omega_m H_0^2}{8\pi} \sum_j^N \Delta_m(\mathbf{x}'_j) \frac{(\mathbf{x}_i - \mathbf{x}'_j)}{|\mathbf{x}_i - \mathbf{x}'_j|^3}. \quad (4)$$

The summation is done up to a distance of $150h^{-1}\text{Mpc}$.

The gravitational force induced by the different cosmic web morphological components is obtained by the straightforward mass-weighted summation over all gridpoints that are located within the NEXUS+ identified regions, ie. the regions identified by NEXUS+ with either cluster node, filament, wall or void. The four cosmic web morphological components are assigned by index CWM = *node, fil, wall, void*. The (peculiar) gravitational force induced by the mass residing in any of these four morphological components is then the sum of the gravitational pull induced by the M mass elements residing in the corresponding areas,

$$\mathbf{g}^{\text{CWM}}(\mathbf{x}_i) = \frac{3\Omega_m H_0^2}{8\pi} \sum_k^M \Delta_m(\mathbf{x}'_k) \frac{(\mathbf{x}_i - \mathbf{x}'_k)}{|\mathbf{x}_i - \mathbf{x}'_k|^3}. \quad (5)$$

where \mathbf{x}_i is the location for which the force is calculated, \mathbf{x}_k one of the locations identified as belonging to morphological feature CWM and M the total number of grid-points identified with that morphological feature.

The net result of the force calculation is a representation of the force field $\mathbf{g}(\mathbf{x})$ at every gridpoint by five force vectors, the full gravitational force $\mathbf{g}(\mathbf{x}_i)$, and the four morphological contributions, $\mathbf{g}^{\text{node}}(\mathbf{x}_i)$, $\mathbf{g}^{\text{fil}}(\mathbf{x}_i)$, $\mathbf{g}^{\text{wall}}(\mathbf{x}_i)$ and $\mathbf{g}^{\text{void}}(\mathbf{x}_i)$. Evidently, the total force $\mathbf{g}(\mathbf{x}_i)$ is the sum of the four morphological contributions,

$$\mathbf{g}(\mathbf{x}_i) = \mathbf{g}^{\text{node}}(\mathbf{x}_i) + \mathbf{g}^{\text{fil}}(\mathbf{x}_i) + \mathbf{g}^{\text{wall}}(\mathbf{x}_i) + \mathbf{g}^{\text{void}}(\mathbf{x}_i). \quad (6)$$

3.1.1 Gravitational Force field: visualization

One of the principal aspects of the present study is to study and assess the gravity, velocity and tidal tensor fields. Before any quantitative and statistical assessment of these fields, the most direct impression of their characteristics and spatial properties is obtained by visual inspection.

To obtain an impression of the spatial structure and properties of the gravity and velocity fields, we invoke a few different visualisations:

- *gravitational force amplitude maps*

of the amplitude of the gravitational force, and of the amplitude contributions by the various individual cosmic web morphological components.

- *gravity vector field maps*

This includes maps of the full gravity vector field, as well as the vector plots of the gravity contributions by the various individual cosmic web morphologies.

In the various gravity vector plots, we depict the component of the gravity vector in the plotted (2-D) box slice. The vectors are oriented towards the direction of the gravity vector component in the box slice. The length of the gravity vectors is normalized in one of two different options:

- *total gravitational force:*

vector length proportional to the amplitude of the total gravitational force $\mathbf{g}(\mathbf{x})$, in units of the mean gravitational force amplitude, ie. in units of the dispersion $\sigma(|\mathbf{g}|)$.

$$\mathbf{g}_{\text{tot}}^{\text{CWM}}(\mathbf{x}) = \frac{\mathbf{g}^{\text{CWM}}(\mathbf{x})}{\sigma(|\mathbf{g}|)}. \quad (7)$$

- *relative gravitational force:*

local relative contribution to the gravitational force by each of the cosmic web components, by expressing the amplitude of the gravitational force in terms of the (local) total gravitational force $\mathbf{g}(\mathbf{x})$,

$$\mathbf{g}_{\text{rel}}^{\text{CWM}}(\mathbf{x}) = \frac{\mathbf{g}^{\text{CWM}}(\mathbf{x})}{|\mathbf{g}(\mathbf{x})|} = \frac{\mathbf{g}_{\text{tot}}^{\text{CWM}}(\mathbf{x})}{|\mathbf{g}_{\text{tot}}(\mathbf{x})|}. \quad (8)$$

In a sense, $\mathbf{g}_{\text{rel}}^{\text{CWM}}(\mathbf{x})$ adheres to the concept of the fractional contribution by the cosmic web components CWM to the local gravitational force.

- *velocity streamline map.* The velocity streamline field provides a transparent view of the spatial structure of the velocity field, and allows the identification of regions dominated by divergence, ie. inflow or outflow, and those by shear flow. To this end, the gravity field is transformed into an *equivalent* linear velocity field (Peebles 1980),

$$\mathbf{v}_{\text{lin}} = \frac{2f}{3H_0\Omega_m} \mathbf{g}, \quad (9)$$

in which the linear growth rate

$$f(\Omega_m) = \frac{a}{D} \frac{dD}{da} \approx \Omega_m^\gamma, \quad \gamma = 0.55 + 0.05(1+w), \quad (10)$$

Streamlines are everywhere tangent to the velocity vectors in the flow field, and represent the direction of velocity at each point in the flow. On the basis of the linear velocity field, the streamline map is inferred using the matplotlib (Hunter 2007) function `pyplot.streamplot`.

3.2 Tidal field

To calculate the tidal field at $\mathbf{r} = (x_1, x_2, x_3)$ we use the traceless tidal tensor defined as (van de Weygaert & Bond 2008b)

$$T_{ij}(\mathbf{r}) = \frac{3\Omega_m H_0^2}{8\pi} \int d\mathbf{r}' \Delta_m(\mathbf{r}') \frac{3(x'_i - x_i)(x'_j - x_j) - |\mathbf{r}' - \mathbf{r}|^2 \delta_{ij}}{|\mathbf{r}' - \mathbf{r}|^5} - \frac{1}{2} \Omega_m H_0^2 \Delta_m(\mathbf{r}) \delta_{ij}, \quad (11)$$

In order to calculate this numerically we turn the integral into a discrete sum over the grid with the DTFE density field values. In our evaluations, we smooth the density field with a Gaussian on a scale of $5 h^{-1} \text{Mpc}$. This is done to smooth out the regions in which nonlinear behaviour would be dominant. Representing this field on a discrete grid, the tidal force integral expression is converted into a sum over the mass-weighted contribution to the tidal force by each gridpoint. Evaluating the tidal field at the gridpoint (\mathbf{r}), the corresponding grid expression for the full tidal field $\tilde{T}_{ij}(\mathbf{r})$ is the sum over all N gridpoints (\mathbf{r}')

$$\tilde{T}_{ij}(\mathbf{r}) = \frac{3\Omega_m H_0^2}{8\pi} \sum_k^N \Delta_m(\mathbf{r}') \frac{3(x'_i - x_i)(x'_j - x_j) - |\mathbf{r}' - \mathbf{r}|^2 \delta_{ij}}{|\mathbf{r}' - \mathbf{r}|^5}. \quad (12)$$

In order to separate the tidal field contribution by the different components CWM - (node, filament, wall or void) - of the cosmic web we sum only over the M gridpoints that are located within a region identified as of morphology CWM. Only the mass allocated at those gridpoints is taken along in the tidal force calculation.

$$\tilde{T}_{ij}^{\text{CWM}}(\mathbf{r}) = \frac{3\Omega_m H_0^2}{8\pi} \sum_k^M \Delta_m(\mathbf{r}') \frac{3(x'_i - x_i)(x'_j - x_j) - |\mathbf{r}' - \mathbf{r}|^2 \delta_{ij}}{|\mathbf{r}' - \mathbf{r}|^5}. \quad (13)$$

The sum uses all cells up to a radius of $150h^{-1} \text{Mpc}$. The traceless tidal tensor T_{ij} follows from

$$T_{ij} = \tilde{T}_{ij} - \frac{1}{3} (\tilde{T}_{11} + \tilde{T}_{22} + \tilde{T}_{33}) \delta_{ij}. \quad (14)$$

The eigenvalues of tensor T_{ij} are

$$T_1 > T_2 > T_3 \\ |T| = \sqrt{T_1^2 + T_2^2 + T_3^2} \quad (15)$$

where T_1, T_2 and T_3 are the sorted eigenvalues of the T_{ij} matrix and $|T|$ signifies the strength of the tidal field. The accompanying eigenvectors $\hat{T}_1, \hat{T}_2, \hat{T}_3$ are sorted accordingly. The value of the different eigenvalues signify the level of elongation or contraction that the corresponding mass element undergoes due to tidal forces.

3.2.1 Tidal field: normalization & visualization

In the analysis of the tidal field, we use two different normalization options:

- *total* tidal force:

the tidal force induced by cosmic web component CWM, $T_{ij}^{\text{CWM}}(\mathbf{x})$, in units of the mean tidal force amplitude, ie. the dispersion $\sigma(|T|)$

$$T_{ij,\text{tot}}^{\text{CWM}}(\mathbf{x}) = \frac{T_{ij}^{\text{CWM}}(\mathbf{x})}{\sigma(|T|)}. \quad (16)$$

- *relative* tidal force:

local relative contribution to the tidal force by each of the cosmic components, by expressing the tidal tensor components and amplitude in terms of the local total gravitational force $|T|_{\text{tot}}(\mathbf{x})$,

$$T_{ij,\text{rel}}^{\text{CWM}}(\mathbf{x}) = \frac{T_{ij}^{\text{CWM}}(\mathbf{x})}{|T|(\mathbf{x})}. \quad (17)$$

In a sense, $T_{ij,\text{rel}}^{\text{CWM}}(\mathbf{x})$ adheres to the concept of the fractional contribution by the cosmic web components CWM to the local tidal field.

To visualize orientation, coherence and strength of the tidal force field, we use two different kinds of maps:

- *tidal force amplitude maps*

maps of the amplitude of the tidal field and tidal field contributions by the various cosmic web morphological components. For the amplitude of the tidal field we use $|T|$ as defined in Eq. 15.

- *tidal bar maps*

Tidal bars indicate the direction of the principal orientation of the tidal force field, in combination with their strength. They have the orientation of the eigenvectors of the tidal force, with a length proportional to the absolute value of the corresponding eigenvector,

$$T_{i,\text{plot}} = \hat{T}_i |T_i|. \quad (18)$$

In the tidal bar maps in the present study we depict the compressional component of the tidal force.

From these maps we may hence deduce the directions along which the mass elements get compressed.

4 GRAVITATIONAL FORCE FIELD

The gravity field contributions by the various cosmic web components, for the specific case of the slice in figure 4, are shown in figure 6 and figure 7. The four panels in figure 6 show the gravity vectors for the combined force impact by filaments (top lefthand frame), voids (top righthand frame), walls (bottom lefthand frame) and cluster nodes (bottom righthand panel). We should note that the vector arrows for the filament force field are rescaled, as they are by far the most substantial contribution to the gravity force field (which should perhaps not surprise us, given filaments contain more than 50% of the cosmic matter content, see Cautun et al. (2014)). With the gravity vector plot providing insight into the structural patterns of the induced gravitational force fields, maps of the strength of the gravitational force yield the needed information on the relative strength of their influence. Figure 7 contains the four corresponding panels with force amplitude level maps for the filament population (top lefthand), void population (top righthand), wall population (bottom lefthand) and cluster nodes (bottom righthand).

One immediate observation is the significant differences between the gravitational influence of the different morphological components of the cosmic web. Each contributes uniquely to the total force field, yielding force fields that differ substantially in shape, coherence, scale and amplitude. Most outstanding is the dominant gravitational influence of the filamentary network. Their overarching strength can be directly inferred from the gravity amplitude maps in figure 7. The towering influence of filaments is expressed in the fact that throughout the simulation box the filament force is factors higher than that exerted by voids and walls. Only cluster nodes reach comparable strengths, but this is only restricted to the immediate vicinity of the cluster nodes. Perhaps the most interesting finding is that of the significant and coherent gravitational impact of voids, marked by a typical signature in terms of characteristic bubble shaped regions in and around minima in the matter distribution, the manifestation of a typical - effectively repulsive - force field pattern. Moreover, comparison between the cluster node and void force field reveals the perhaps surprising conclusion that voids are the more dominant component over far larger regions of a cosmic volume.

4.1 Filaments

From the filament force vector field map (top lefthand panel, fig. 6), we see that the gravitational influence of filaments acts coherently over a large range of distances. In fact, its overall structure and pattern is quite close to that of the total gravitational force field (bottom panel, fig. 4, a telling testimony of the fact that most of the large scale gravitational force field is due to the combined influence of the filamentary network. We should also note that, as expected, the force field only traces the largest structures. Small scale features hardly induce a noticeable effect. The overpowering dynamical influence of the filamentary network should not come as a surprise: the filamentary network of the cosmic web represents more than 50% of the cosmic matter content of the universe (Cautun et al. 2014). As important is the pervasive spatial character of the multiscale filamentary network, with filaments spreading throughout cosmic volumes and their tendrils branching out into even the most remote and desolate realms (voids).

Inspection of the force amplitude map shows that over nearly the entire cosmic volume filaments are responsible for high force amplitudes, their overdense nature guaranteeing a consistent and coherent cumulative attractive force contribution (top lefthand panel, fig. 7). We find that over almost 97% of the cosmic volume, the filament induced forces dominate over that induced by any of the other morphological components (table 2, 3rd column). The largest and densest filaments create coherent force fields on scales up to $\sim 50 h^{-1} \text{Mpc}$. In fact, the coherence scale of the force field is much larger than that of the weblike structure of the underlying matter distribution.

4.2 Voids

The picture is considerably different for the void force field. The top righthand panel of figure 6 shows a spatial pattern marked by individual divergent patches, indicating individual expanding void regions. Inside these individual void regions, the force field increases monotonically - and usually almost linearly - from the center of a void to their boundary of surrounding walls and filaments. It produced the characteristic superhubble expanding void regions (see e.g. Icke 1984; van de Weygaert & van Kampen 1993). Due to the rapidly rising mass density near their boundary, the strength of the void force

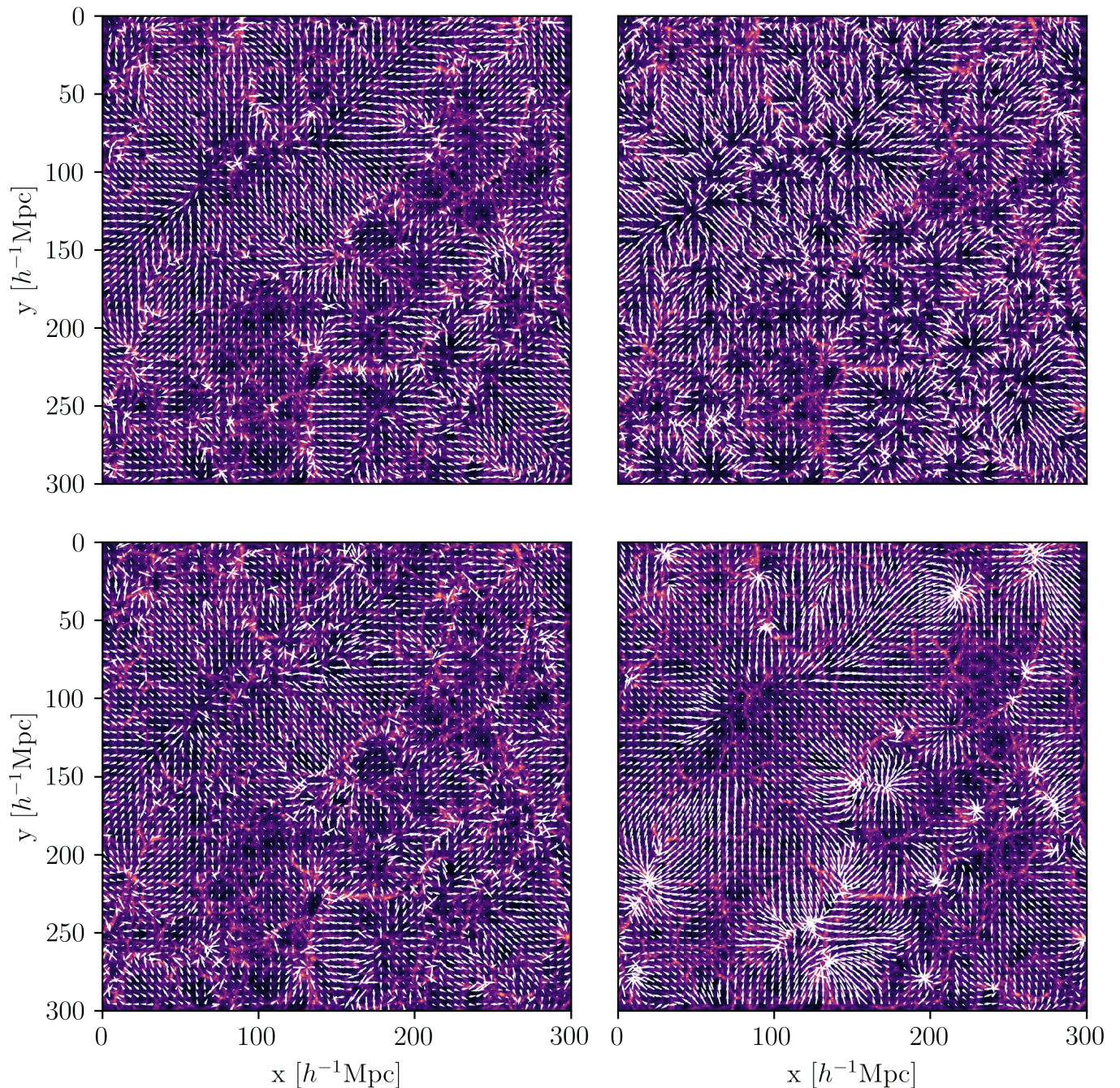


Figure 6. Gravitational Force field by Cosmic Web component: vector field. The force fields originating of the different components for the complete field, normalised by the total field (see Section 3.1.1). Top left has filaments, Top right has voids, bottom left has walls and bottom right has nodes. **Note:** For this figure, filaments are rescaled with respect to the other components. In comparison the filament arrows should be longer. Voids, walls and nodes are one the same scale.

field drops at the void edge, resulting in the conspicuous bubble-like configurations that stand out in the void force field in figure 6.

Overall the void force field appears to be one in which individual superhubble expanding voids (Icke 1984) produce a segmented volume with clearly distinguishable individual void regions. Indicative for the latter are the small voids near the center, whose influence appears to be mainly limited to their own interior. Nonetheless, we may observe assemblies of voids that seem to operate collectively in pushing out the surrounding mass, such as the the void agglomera-

tion at the top left of the field. Its force fields adds up to create an expanding region on a scale of $\sim 50 h^{-1}\text{Mpc}$.

In all, it suggests that in general voids hold sway over in particular their local environment, in which large scale effects are significant but less prominent than those seen in the filament force field. On large scales voids do produce significant residual large scale effects emanating due to their spatial clustering, be it of a lower amplitude than that characteristic for the forces in individual voids. It confirms

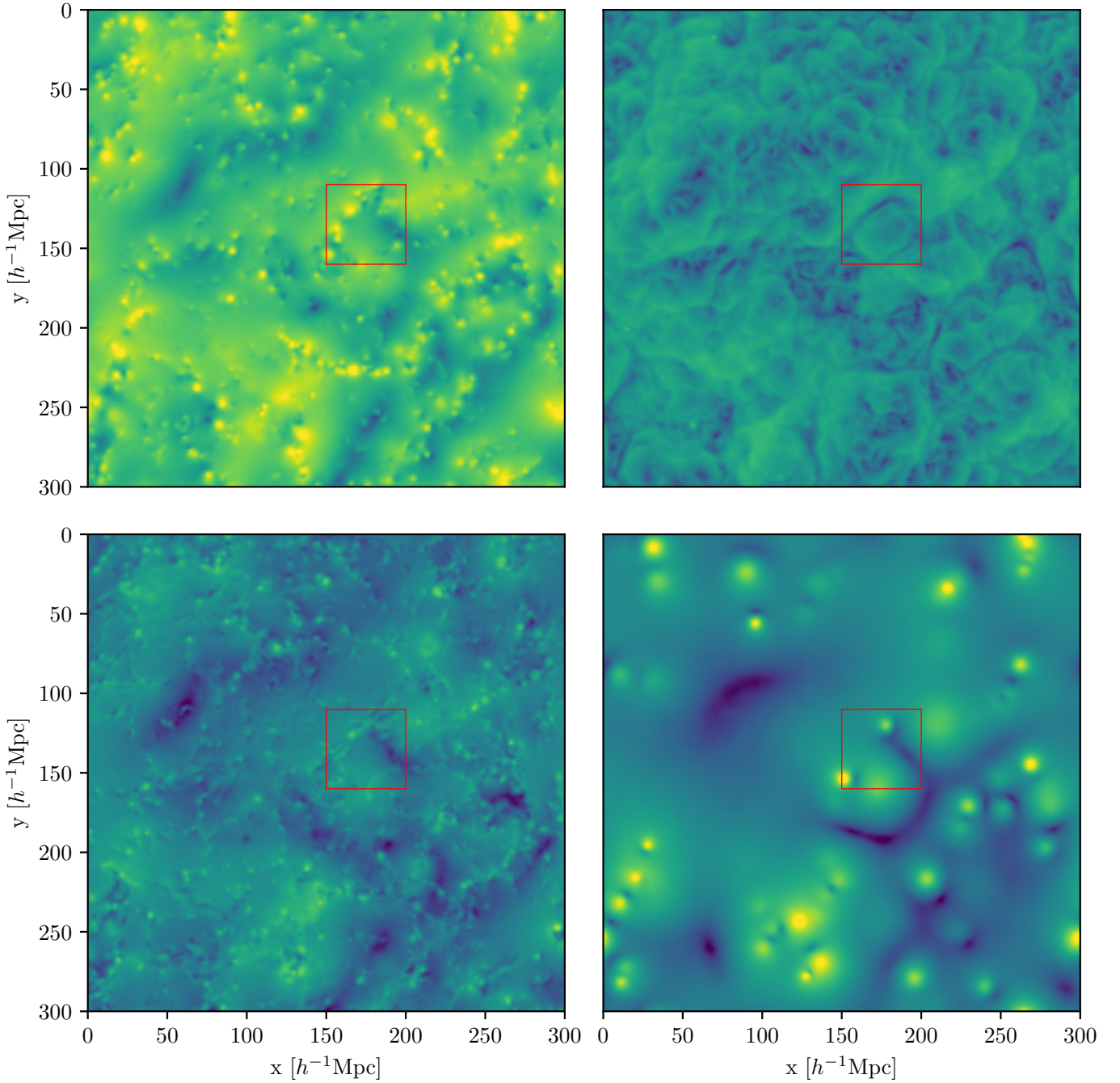


Figure 7. Gravitational Force field by Cosmic Web component: amplitude field. The amplitude of the peculiar force field $\log_{10} |\mathbf{g}|$ for the different components of the cosmic web for a $300 h^{-1}\text{Mpc}$ by $300 h^{-1}\text{Mpc}$ by $0.59 h^{-1}\text{Mpc}$ slice. The top left panel shows the component originating from filaments, the top right panel shows the component originating from voids, the bottom left panel shows the component originating from walls and the bottom right panel shows the component originating from nodes. The red box indicates the region used for the zoom in Figure 10.

the finding by [Platen et al. \(2008\)](#), who showed that voids even induce noticeable tidal effects over scales in excess of $\sim 30 h^{-1}\text{Mpc}$.

4.3 Walls

The force field induced by the walls is the least conspicuous one of the web morphologies. Throughout the cosmic volume it is very weak, as testified by the map of its force strength (see bottom lefthand panel fig. 7. The walls do not contribute much to the overall force

field. Also, as they populate moderate density realms as well as the interior of voids (see e.g. [Cautun et al. 2014](#)), their effect may be effectively either be attractive or repulsive. To some extent, it leads to the moderate and low density walls compensating each others force contributions. It results in a force field that only faintly reflects the cosmic web pattern seen in the filament and void force fields.

Globally, the spatial structure of the wall force map bears resemblance to that of the filament strength map (top lefthand panel fig. 7. It appears to be a faint reflection of the filament strength map. One

may recognise only a part of the most prominent features that are seen in the filament force field, others are conspicuously absent: e.g. the strong filament force field at the top lefthand corner of the box does not seem to have a wall equivalent. Also the overall large scale pattern of the wall force vector map does resemble that of the filament force vector map. However, the wall force map appears far less coherent and organised, marked by a considerable number of randomly scattered small scale patches of irregular oriented force vectors.

4.4 Cluster Nodes

A rather surprising finding is the fact that cluster nodes only appear as highly localised force centers, and they are far from the dominant gravitational component of the cosmic web that we had expected them to be.

In the force strength map (bottom righthand panel, fig. 7) cluster nodes stand out as compact high amplitude peaks in the force field. They act as a set of randomly clustered monopole attractors. The cluster nodes are only dominant over the rather small scales of their immediate environment. At this range, they overshadow all other force contributions. In most cases, this is only over distances of a few $h^{-1}\text{Mpc}$, in an occasional exception out to $\sim 20h^{-1}\text{Mpc}$. The latter concerns an agglomerate, “superclusters”, such as that at the bottom centre of the map (bottom righthand panel, fig. 7).

Their spatial connection to the cosmic web is less clear, and it is not easy to recognize the global weblike mass distribution in their own spatial arrangement or the direct dynamical relation between the cluster nodes and the spatial intricacies of the cosmic web. At large scales there are substantial regions where the influence of multiple nodes is one in which they effectively cancel each other, resulting in a contribution that is less than - or at best comparable to - that by the voids.

4.5 Gravity Field strength: statistical analysis

To quantify the visual impressions of the force field contributions by the different cosmic web components, discussed extensively above, we assess the statistical (volume-weighted) distribution of the fractional gravitational force contributions by each of the cosmic web components *CWM*. The fractional gravitational force $\mathcal{F}(\mathbf{r})$ at each location \mathbf{r} is defined by the ratio,

$$\mathcal{F}^{\text{CWM}}(\mathbf{r}) = \frac{|\mathbf{g}^{\text{CWM}}(\mathbf{r})|}{|\mathbf{g}_{\text{tot}}(\mathbf{r})|}, \quad (19)$$

where $\mathbf{g}^{\text{CWM}}(\mathbf{r})$ is the gravitational force exerted by the components *CWM* - i.e. filaments, voids, walls and cluster nodes - at location \mathbf{r} . The total sum of these is

$$\mathbf{g}_{\text{tot}}(\mathbf{r}) = \sum_{\text{CWM}} \mathbf{g}^{\text{CWM}}(\mathbf{r}). \quad (20)$$

Note that the ratio is independent of direction, while the sum of the forces does take into account the orientation of each force contribution. As a result, the fractional force $\mathcal{F}(\mathbf{r})$ may have a value larger than unity. The average ratios for the fractional force contributions are listed in table 2. There is a clear hierarchy of force field contributions: filaments \gg voids $>$ nodes $>$ walls. Averaged over all volume elements, the filament impact is on average no less than 60%, with voids as a surprising second at on average contributing $\sim 20\%$ of the local gravitational force.

The distribution for the complete force field is shown in the top

Table 2. Gravitational Force Statistics. The second column shows the mean force ratio for the different components of the cosmic web, Note the direction dependence in the ratio $|\mathbf{g}|^{\text{CWM}}/|\mathbf{g}|^{\text{tot}}$. The third column shows the percentage of the total volume where each component has a contribution that is larger than the other components.

Component	Mean [%]	Largest in [%]
Filaments	60.4	97.2
Voids	20.3	0.9
Nodes	17.0	1.5
Walls	13.7	0.4

panel of Figure 8. The bottom four panels show the same distribution, but split up by morphology. They show for each of the four cosmic web environments, the fractional force contribution by each of the morphologies. In other words, these tell you what the relative impact is of filaments in voids, of voids in filaments, or of cluster nodes in filaments.

The top panel of Figure 8 reveals the major differences in force impact by the different cosmic web components. Filaments stand out as by far the most dominant element of the cosmic web. Their force impact ranges over a wide range of values $\mathcal{F}^{\text{fil}}(\mathbf{r})$, centering around 60% of the total gravitational force. At the vast majority of locations the filamentary cosmic web is the leading gravitational influence.

The role of voids is one of the most interesting aspects of the gravitational force inventory. They appear to be the second most dominant source of gravitational force. They account for more than 20% of the local force at far more locations than e.g. walls, and even than cluster nodes. At many locations voids assume an even stronger fraction of the force budget. The fact that the void distribution function has a long high end tail implies that voids are the dominant influence at various regions of the cosmic web. Nearly without exception this concerns the interior of large voids. A similar long high end tail is found for the cluster node gravitational influence $\mathcal{F}^{\text{node}}(\mathbf{r})$, reflecting the overpowering gravitational influence of nodes in and around their own location. We find that the cluster node distribution has a mode near 10 – 12% of the total force, substantially less than that of voids. It means that over most of the cosmic volume, voids have a stronger gravitational influence than cluster nodes !

As expected, the distribution of the wall force fraction $\mathcal{F}^{\text{walls}}(\mathbf{r})$ expresses their weak role in the cosmic web force budget. Not only does the distribution peak around 10%, quite similar to the mode for cluster nodes, but it also concerns a narrow distribution without an outstanding tail towards higher values. It shows that walls, over nearly the entire cosmic volume, are only a minor fiddle in the force concert.

Assessing the force impact differentiated by cosmic web environment provides additional information on the nature of the dynamical impact of filaments, voids, walls and nodes. These are provided by the bottom panels of figure 8 and by the panels of figure 9.

Differentiating between the impact of morphological components in different environments, the four bottom panels of figure 8 reveal a few interesting aspects. Filaments are clearly the dominant dynamical component over the entire cosmic volume, and this is true in voids, walls as well as in filaments themselves (voids: bottom lefthand panel fig. 9, walls: bottom righthand panel fig. 9, filaments: top righthand panel fig. 9). In the case of the filament interior, the shoulder of the filament pdf reveals that it is in particular inside filaments themselves that they display the strongest impact: filaments hold sway inside filaments. A minor detail is that we see that $\mathcal{F}^{\text{fil}}(\mathbf{r})$ is higher in

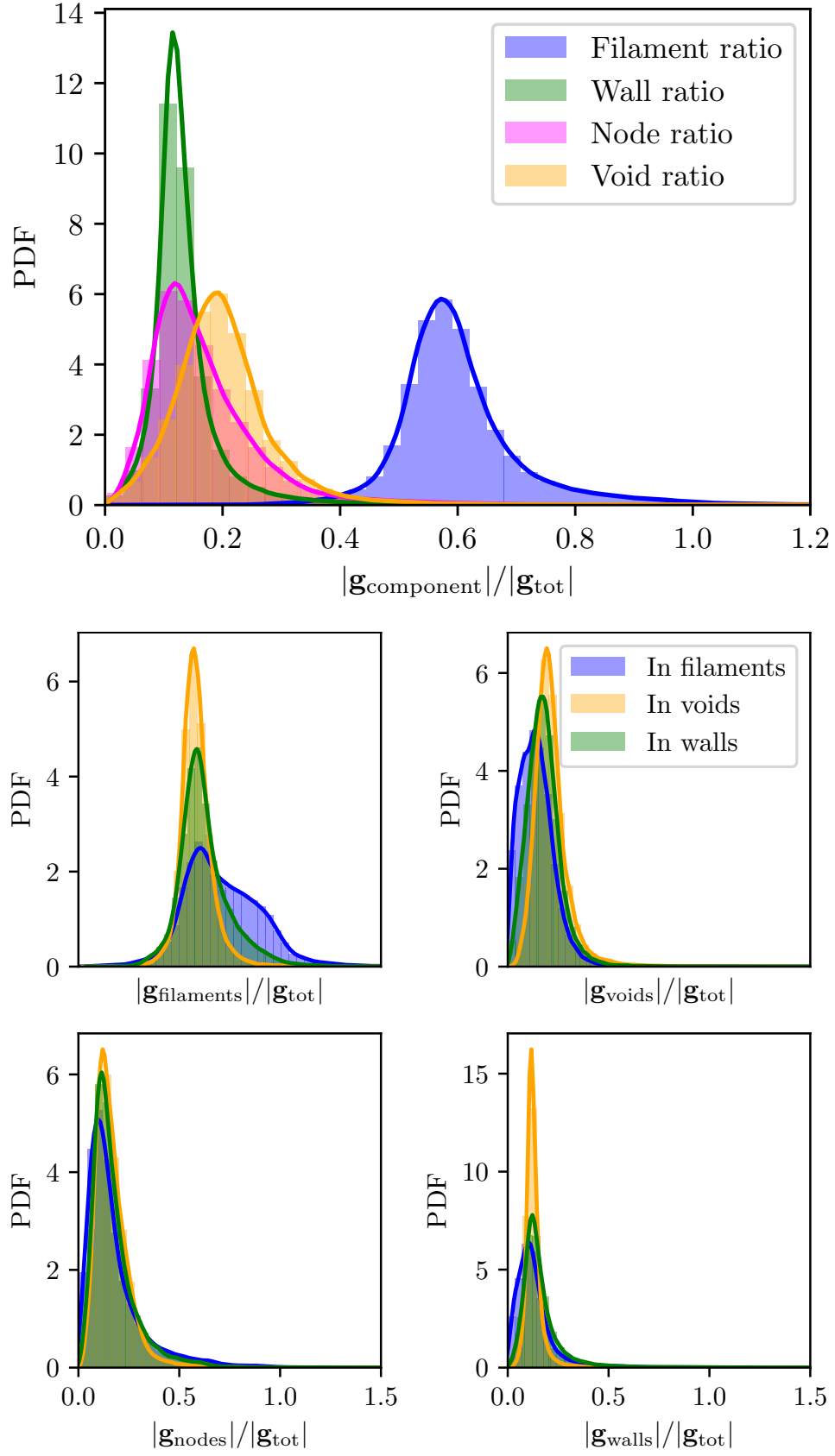


Figure 8. Cosmic Web Gravitational Force Field: Strength Inventory. Top panel: The distribution of $|\mathbf{g}^{\text{CWM}}|/|\mathbf{g}_{\text{tot}}|$ for the different components of the cosmic web. Each using the complete field. Bottom four panels: the distribution of $|\mathbf{g}^{\text{CWM}}|/|\mathbf{g}_{\text{tot}}|$ for the different components of the cosmic web. Per panel the pdf for cosmic web component CWM is plotted, with three different environments: filaments (blue), voids (yellow), walls (green). Centre left: filament induced force field. Centre right: void induced force field. Bottom left: wall induced force field. Bottom right: cluster induced force field.

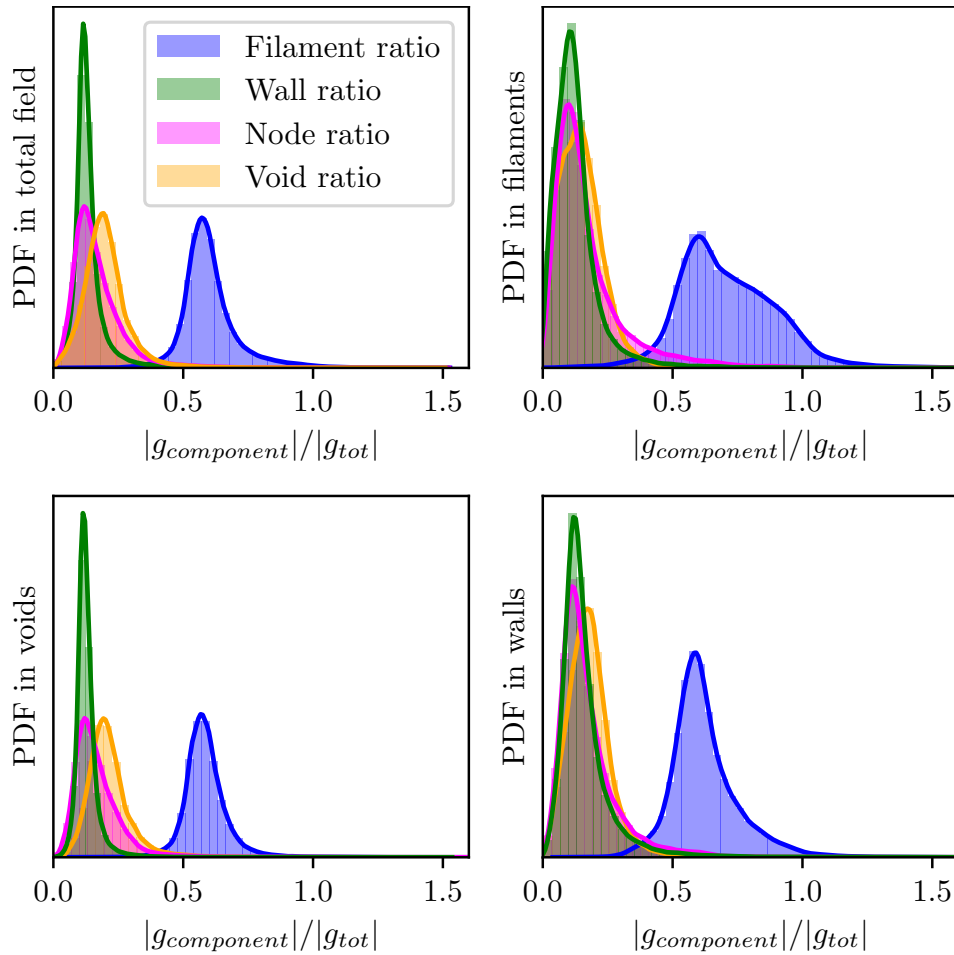


Figure 9. Cosmic Web Gravitational Force Field: Strength Inventory by Cosmic Web environment. The panels show the pdf of the induced gravitational force field $|g^{CWM}|/|g_{tot}|$ by each of the four cosmic web components CWM in the different cosmic web environments. The different colours represent the different components: filament induced force field (blue), void induced force field (yellow), wall induced force field (green) and cluster node induced force field (magenta). Top left panel: total gravitational field. Top right panel: gravitational field in filaments. Bottom left panel: gravitational field in voids. Bottom right panel: gravitational field in walls.

walls than in voids. This surely is a manifestation of the spatial proximity of filaments to these structures: voids are large, and in the central interior the filament’s force may be somewhat weaker than in and around the walls to which they are connected.

For the impact of voids in different cosmic web environments, we see that they hold their strongest influence over the void regions themselves, while they are relatively stronger in walls than in the interior of filaments (centre righthand panel fig. 8). Inside void interiors, the force inventory quantified in the bottom lefthand panel of fig. 9 shows how important external influences are in the dynamics and evolution of voids. The filament forces dominate the force field of voids. This is certainly true for the outer regions of voids, but may even be so for their inner regions. The latter will be most evident for small voids, where these external forces may even induce their collapse, an essential process - called void-in-cloud - in the buildup of the void population (Sheth & van de Weygaert 2004). However, the filaments represents the principal gravitational influence for even the large voids. This implies that any analysis of void dynamics should include the mass distribution surrounding the void (see e.g van de Weygaert 2016, for a recent review), while any exploitation of the characteristics of the void population for cosmological purposes cannot ignore this fact and base their analysis on simplistic isolated

void dynamics (see e.g. Pisani et al. 2019). A recent study of the dynamics of a sample of voids from SDSS, including velocity flow information from the Cosmicflows-4 galaxy peculiar velocity survey, did also indicate this finding in the observational reality (Courtois et al. 2023).

Meanwhile, less outstanding are the observations with respect to the gravitational influence of nodes and walls. Their impact appears relatively indifferent to the environment. The node force fraction decreases slightly going from voids to walls to filaments. This might be somewhat counter intuitive, but is an expression of the fact that filaments are so much stronger than walls and voids. Relatively speaking, nodes will then assume a smaller force fraction $\mathcal{F}^{node}(\mathbf{r})$ in a filament environment.

5 GRAVITATIONAL FORCE FIELD: INDIVIDUAL STRUCTURES

In this section we zoom in on the force structure in and around a few representative individual features. This with the intention to develop an intuitive and visual image of the role and gravitational influence of the different cosmic web components with respect to the various large scale environments, and to appreciate the complex interplay between

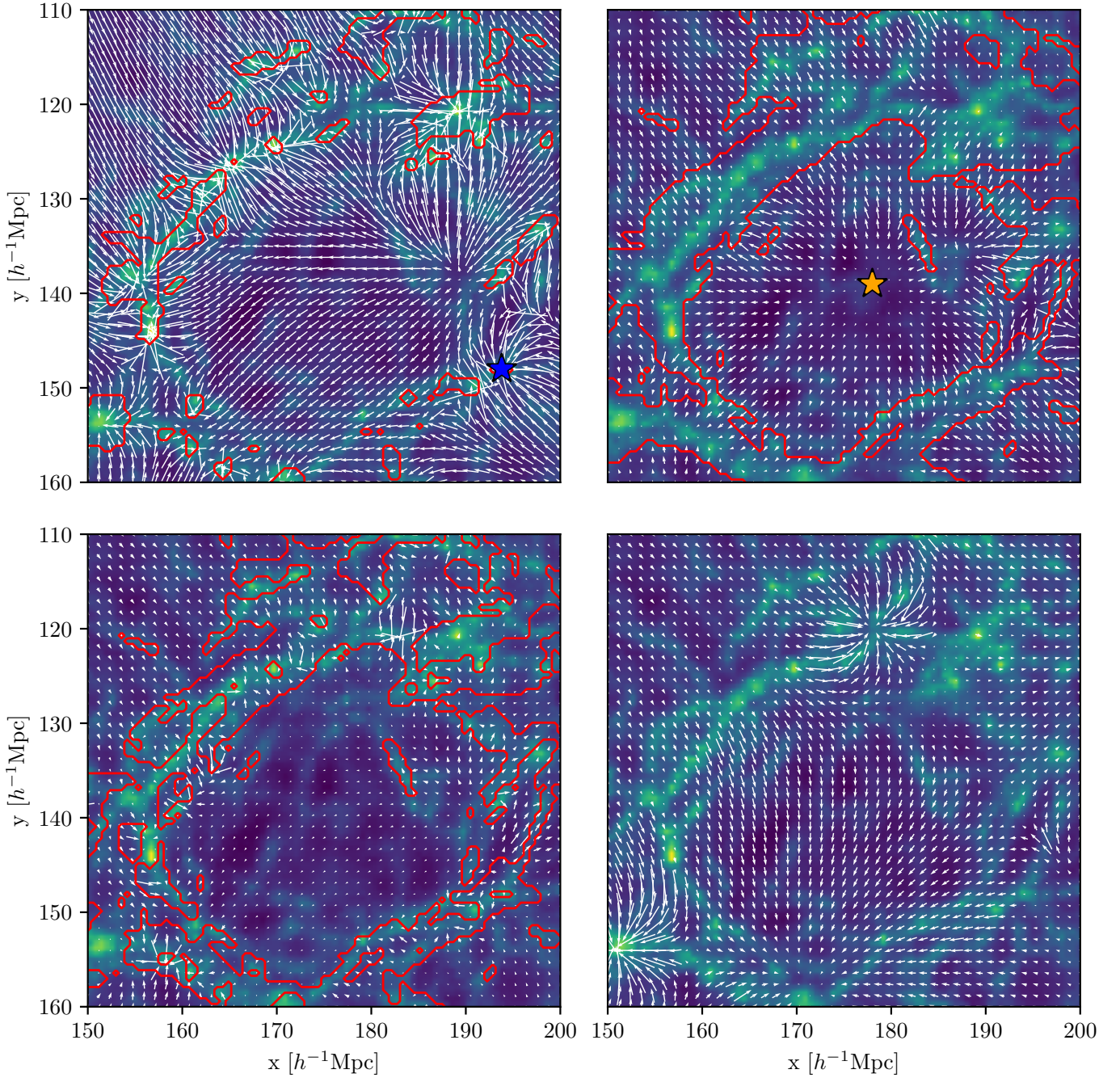


Figure 10. Gravitational force vector field in and around void region. The region is a $50 h^{-2} \text{Mpc}^2$ region centered on a void (void center: orange star, top lefthand panel). The panels represent the force vector field in this region generated by the different morphological components of the cosmic web. Top left panel: filament induced force field; top right panel: void induced force field; bottom left panel: wall induced panel; borrom right panel: cluster node induced field. The arrows show the magnitude and direction of the corresponding (normalized) gravitational force, \mathbf{g}_{tot}^{CWM} . The vector field is superimposed on the (log) density field map. In the different panels the red contours indicate the regions belonging to the corresponding NEXUS+ identified cosmic web component. The orange star (top righthand panel) indicates the void center, the blue star (top left panel) the filament location, around which the radial force profiles in figures 11 and 12 are determined.

them. We concentrate on the force field in and around a single void, around a filament, and one in and around a cluster node. In each case we zoom in on $50 \times 50 h^{-1}$ Mpc segment. They confirm the observations and conclusions that we reached in the previous section on the basis of its structural and statistical assessment analysis of the cosmic web gravitational force field.

5.1 Case study 1: void force field

Our first study case is the force field in and around a void. Against the backdrop of the corresponding density field, with the red contours indicating the NEXUS+ identified region, the four panels in figure 10 show the decomposition of the gravitational force field in and around the void into its individual morphological contribu-

tions. The force field is decomposed into the filament induced force field (top lefthand panel), that by voids themselves (top righthand panel) by walls (bottom lefthand panel) and by cluster nodes (bottom righthand panel).

Evidently, the filament induced force field dominates over nearly the entire region. Two of the most characteristic aspects of the filament induced force field is its large scale reach and coherence, and the easily recognisable signature shear pattern in the gravity vector field. The latter involves the splitting of the gravity vector field in opposite directions at saddle points of the corresponding gravitational potential. Two of the most outstanding ones are the one near righthand edge of the void (at $(x, y) \approx (190, 140)h^{-1}\text{Mpc}$, and the one near $(x, y) \approx (170, 120)h^{-1}$. The latter is situated in between two dense concentrations within the filamentary network. These are responsible for stronger attractive cores along the filaments. The two dense mass concentrations along the filament turn out to be massive filamentary branches connecting to a cluster node, forming the connections of the cluster with the filamentary skeleton of the cosmic web. Over this specific void, the cluster node represents a sizeable external influence over the entire realm of the void. The cluster induced force field is comparable in magnitude to that of the void force field itself.

The coherence of the filament induced gravity field over the entire reach of the central void is the source for a large scale bulk flow (eq. 9), superimposed on the iconic superhubble divergent flow induced by the void(s) themselves. The induced force field by the voids themselves is easily recognisable, consisting of an almost pure divergent vector field centered around the density minimum (top righthand panel fig. 10. To first approximation, the superhubble force field in the interior of the void involves a radially outward directed force that increases with distance to the center (see eg. Icke 1984; van de Weygaert 2016). It reflects the almost uniform (underdense) mass distribution in the interior of the void (see e.g van de Weygaert & van Kampen 1993; Sheth & van de Weygaert 2004). In reality, also voids display a substantial level of substructure. The presence of a small expanding subvoid superimposed on the large central void reflects the multiscale structure of both the interior void density and velocity field. It is the product of the hierarchical buildup of the void population (Sheth & van de Weygaert 2004; Aragon-Calvo & Szalay 2013).

While the filamentary force field displays a coherence over nearly the entire volume, the void induced field appears to be more restricted in spatial extent. The void gravitational force increases radially outward up to its boundary, at a radius of around $r \approx 10 - 15h^{-1}\text{Mpc}$. At the edge it plummets to an almost negligible influence, as the gravity by the higher density outer realms of the voids kick in to compensate for the influence underdense interiors. Minor residual void forces may be traced in the interstitial boundary regions, yielding the suggestion of the voids pushing matter into the surrounding weblike filamentary and planar structures. Similar patterns are seen to emanate from the surrounding voids. As a result, we get the impression of a void force field segmented into separate void regions. This was also seen on the more global scale of the simulation volume in the void force field in figure 6 (top righthand panel). In all, we may conclude that while voids may have some minor effect on large scale flows, their main impact seems to be that of the local pushing around of matter into the interstitial elements of the cosmic web.

Quantitatively the above impressions are supported by the radial profile of the different force amplitudes around the center of the void. The top panel of Figure 13 plots the radially averaged force amplitude as seen from the center of the void. It confirms the dominance of the filament induced gravity (blue line), over the entire interior of the

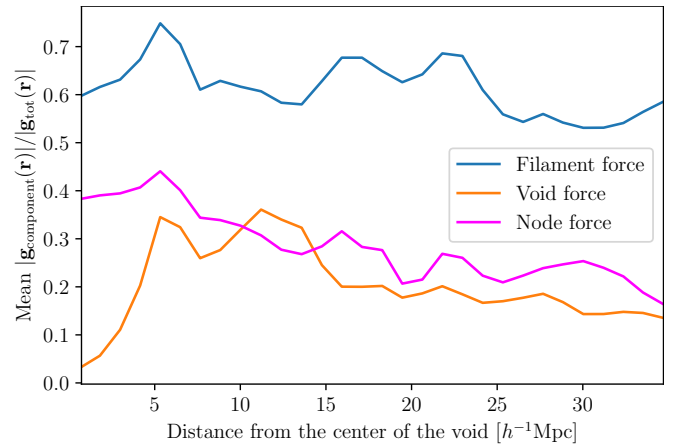


Figure 11. Radial gravitational force (amplitude) profile for the cosmic web components CWM, around the (orange) void center (fig.10 , top righthand panel). Plotted is the force ratio $|\mathbf{g}^{\text{CWM}}|/|\mathbf{g}_{\text{tot}}|$ for the CWM induced gravitational force amplitude, as a function of distance from the void centre. Blue: filament force amplitude; yellow: void force amplitude; magenta: cluster node force amplitude.

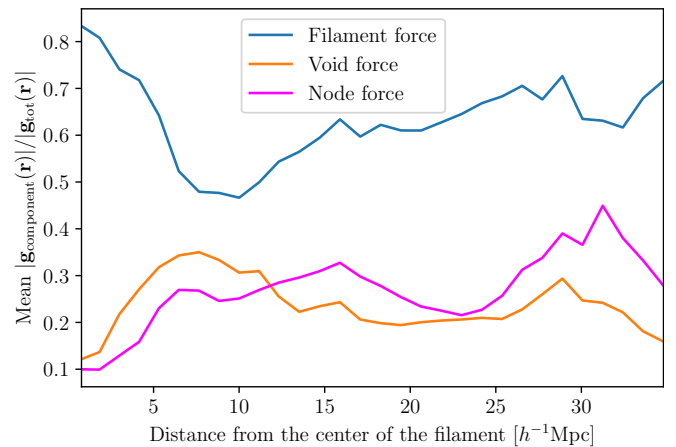


Figure 12. Radial gravitational force (amplitude) profile for the cosmic web components CWM, around the (blue) filament location (fig.10 , top lefthand panel). Plotted is the force ratio $|\mathbf{g}^{\text{CWM}}|/|\mathbf{g}_{\text{tot}}|$ for the CWM induced gravitational force amplitude, as a function of distance from the central filament location. Blue: filament force amplitude; yellow: void force amplitude; magenta: cluster node force amplitude.

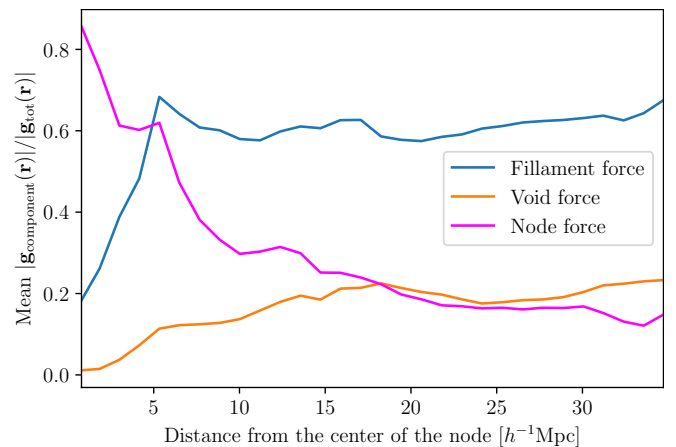


Figure 13. Radial gravitational force (amplitude) profile for the cosmic web components CWM, around the prominent massive cluster in fig. 14. Plotted is the force ratio $|\mathbf{g}^{\text{CWM}}|/|\mathbf{g}_{\text{tot}}|$ for the CWM induced gravitational force amplitude, as a function of distance from the cluster node location. Blue: filament force amplitude; yellow: void force amplitude; magenta: cluster node force amplitude.

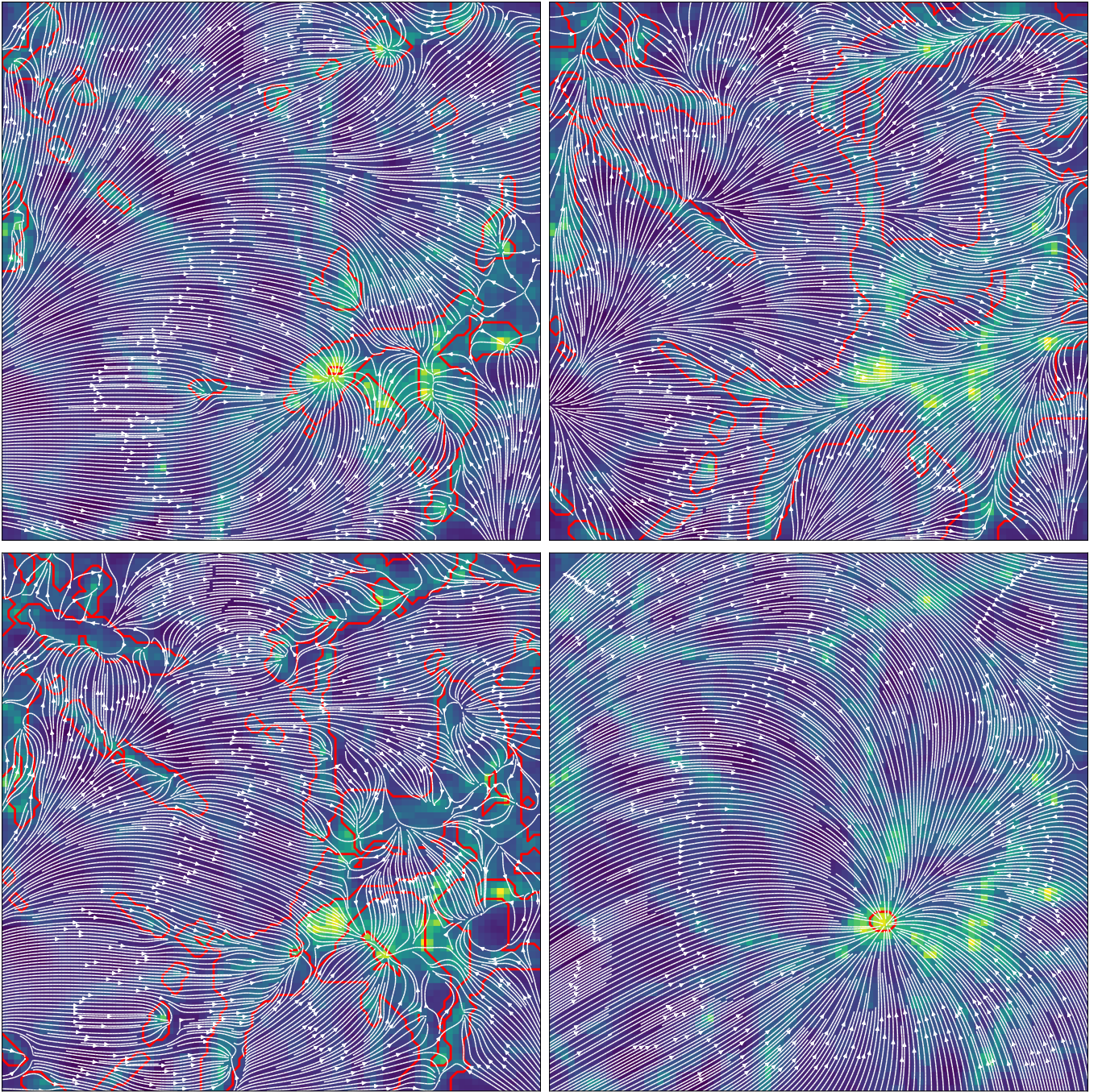


Figure 14. Velocity flow field in and around cluster node. The region is a $50 h^{-2} \text{Mpc}^2$ region, containing a massive cluster node (at bottom righthand corner). The velocity vector field is represented by the corresponding streamlines, highlighting the overall spatial structure of the flowfield. The four panels show the streamline field for the induced velocity flow field by each of the cosmic web morphological components. The velocity field streamlines are superimposed on the (log) density field map. In the different panels the red contours indicate the regions belonging to the corresponding NEXUS+ identified cosmic web component. Top left panel: filament induced velocity field; top right panel: void induced velocity field; bottom left panel: wall induced velocity field; borrom right panel: cluster node induced velocity field. In this individual case, the velocity field is clearly dominated by the cluster.

void (and beyond). The void induced force field (orange line) reveals the expected characteristic (almost) superhubble expansion. Near the edge of the void, the outward directed void force represents a substantial fraction of the complete gravitational force, but never more than around 40% of the filament force. A full account of the force field for this particular voids also includes a substantial influence

from the massive cluster node on its north side, whose magnitude is comparable to that of the void itself. The corresponding force profile (magenta line) confirms the visual impression offered by the bottom lefthand panel of fig. 10.

Seen from the perspective of the filament, a complementary view of the sizeable void influence is obtained. The middle panel of Fig-

ure 13 shows the radial force profile around the dense filament location at the bottom right of the region (marked by a blue star, top left panel fig. 10). At small distances from this location, still inside the filament, the filament induced force field is overwhelmingly dominant, responsible for more than 80% of the full force field. As we move towards the edge of the filament, and enter into the void's realm, we observe a rapid decline in the filament's influence, going along with a corresponding rise of the void's influence. Further afield, as the influence of overdense surroundings at the other side of the void becomes noticeable, we see that the force contribution by the void diminishes while that of filaments remains more or less constant.

5.2 Case study 2: cluster node force field & flowlines

The second case study concerns the force field around an isolated cluster node. To get a visual appreciation of its impact on the environment, we assess the induced flowfield in and around the node. To this end, we use the linear relation between gravity and velocity (Eq. 9). Formally, it is only valid in the linear regime, but to reasonable approximation may also be used in the quasi-linear configurations we are investigating. It yields the implied velocity fields induced by the four different cosmic web components, filaments, voids, walls and cluster nodes. These velocity fields are visualized by means of the corresponding streamlines. It yields a flowline representation of the velocity field that provides a direct insight into the structure of the cosmic migration flows. Figure 14 shows the streamline fields for the induced flowfield by filaments (top lefthand panel), the voids (top righthand panel), the walls (bottom lefthand panel) and the cluster nodes (bottom righthand panel).

The most prominent aspect of the flowfield is the cluster node induced flowfield (bottom righthand panel). The node induced a massive inflow pattern over the entire entire region. The dominant impact of the cluster on its environment is confirmed by the radial force profile centered on the node (bottom panel of fig. 13). In the inner sphere of $\approx 5h^{-1}\text{Mpc}$ around the cluster node, it dictates the gravitational force field, taking care of even more than 80% at its center. Outside of this immediate vicinity, its sway rapidly declines, taken over by the surrounding filamentary web. To a considerable extent, the filament streamlines offer a similar spatial flow pattern, augmented by the presence of shear signature. It concerns the impact of the massive filamentary branches connecting to the node, and as such strongly related to this peak in the mass distribution.

By contrast, the void induced flow field offer a more localized pattern. In the overall pattern we recognize the typical segmented nature of the field, carrying the imprint of individual voids. More so than we have seen in the force vector field, the flow field also reveals the tendency for a large void scale induced bulk flow, running from the lefthand to the righthand side of the region. It is a manifestation of the multiscale nature of the void population, a direct consequence of its hierarchical buildup (Sheth & van de Weygaert 2004; Aragon-Calvo & Szalay 2013). Voids tend to be embedded in larger (less) underdense regions, whose dynamical influence shows up in the superposition of the individual void outflows as a residual large scale (bulk) outflow (see Aragon-Calvo & Szalay 2013, for telling illustrations). As seen from the center of the cluster node, the void induced flow field becomes noticeable at a distance of around $\sim 16h^{-1}\text{Mpc}$, beyond which distance it represents a stronger contribution than that of the cluster itself.

6 TIDAL FIELD

To understand the dynamics underlying the formation and shaping of the cosmic web, tidal gravitational forces and the induced deformation of mass elements play an instrumental role (see e.g. Zeldovich 1970; Bond et al. 1996; van de Weygaert & Bond 2008a; Hahn et al. 2010; Feldbrugge & van de Weygaert 2023, 2024). The present study therefore needs to complement the inventory of the gravitational force in the previous section by an analysis of the corresponding tidal force field.

Following the definitions in section 3.2, in the present study we first investigate the tidal force field generated by filaments, voids, walls and cluster nodes by means of tidal force amplitude maps, i.e. maps of the (traceless) tidal field amplitude $|T|$,

$$|T| = \sqrt{T_1^2 + T_2^2 + T_3^2}, \quad (21)$$

with $T_1 > T_2 > T_3$ the tidal field eigenvalues. Figure 16 presents the tidal amplitude maps for the tidal fields generated by the filament population (top lefthand panel), the void population (top righthand panel), the wall population (bottom lefthand panel) and cluster nodes (bottom righthand panel). The first direct observation from the four frames is the difference between the tidal field morphology and patterns to that of the force field. The tidal force field is intimately linked to the weblike spatial pattern of the cosmic mass distribution, and also reflects more closely its smaller scale structure than the force field. Recent work has also revealed the close similarity between the structure of the primordial tidal field, specifically its eigenvalues, and that of the emerging structure of the cosmic web (see e.g. Feldbrugge & van de Weygaert 2023, 2024).

6.1 Tidal Field illustrated: tidal impact voids

To appreciate the intricacies of the cosmic web tidal force field, it is most insightful to focus on the component induced by the voids and the void population. To this end, we first zoom in on a few interesting and telling regions. Figure 15 shows zoom-ins on four different regions of size $25 \times 25h^{-1}\text{Mpc}$. The four panels show the tidal bars of the compressional components of the tidal field induced by the void population in the matter distribution. The direction of the bars is along the corresponding tidal tensor eigenvectors, their size proportional to that of the corresponding eigenvalues.

The panels illustrate the close connection between the weblike spatial pattern of the matter distribution, and its multiscale nature, and the tidal force field induced by voids, which we find - as discussed in more detail below - to be a surprisingly striking aspect of the large scale tidal field. Even more so than the filament induced tidal force field, we find that the deformation of the matter distribution is strongly correlated to the spatial pattern and connectivity seen in the void induced tidal force field. The void tidal field traces out structures at all scales and over a wide range of densities. It causes compression along even the smaller, more tenuous, structures seen in the density field.

The clearest example of a void's tidal impact is offered by the bottom lefthand panel, centered at the interior of a void. It has the typical characteristics of a tidal force field expected in and around voids. A typical aspect of the void induced tidal force field is that it is weak in the interior of voids. It steeply increases in amplitude as it enters the overdense boundaries, a reflection of the strong differential gravitational force between interior and surroundings. In this sense, it adheres closely to that expected for isolated spherical voids. It induces a compressional component T_{rr} along the radial direction,

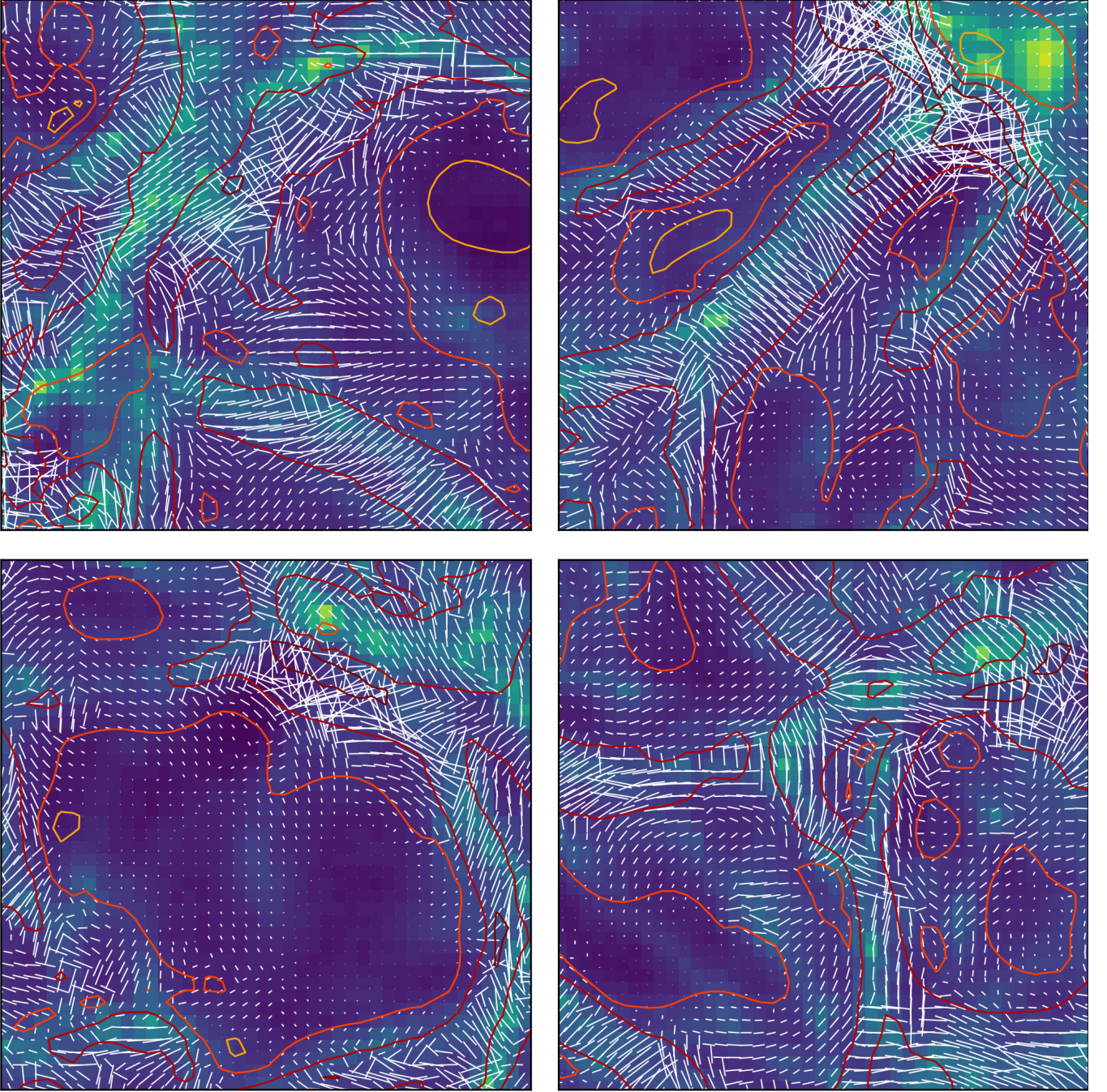


Figure 15. Tidal field induced by voids, in four different $50 h^{-2} \text{Mpc}^2$ regions. The tidal force field is represented by tidal bars and contours. All four panels show the tidal field induced **exclusively** by the void population in the simulation box. The tidal bars and contours are superimposed on the (log) density field map. The tidal bars indicate strength and direction of the compressional component of the tidal field. The definition and construction of the tidal bars is explained in section 3.1.1.

while the dilational components T_{tt} are oriented along the tangential direction. At a radial distance r from the void center, for a void with density profile $\Delta(r)$,

$$T_{rr} = \Omega H^2 [\Delta(r) - \langle \Delta(r) \rangle],$$

$$T_{tt} = -\frac{1}{2} T_{rr}(r), \quad (22)$$

in which $\langle \Delta(r) \rangle$ is the mean interior density of the void. Hence, in the near uniform - bucket shape - mass distribution in the interior

of voids (see e.g. [van de Weygaert 2016](#)) the tidal force field will be negligible. Meanwhile, the fact that $\Delta(r) > \langle \Delta(r) \rangle$ as we enter the boundary of voids implies into a compressional tidal force along the radial direction of the void. It translates into the compression of mass elements in the radial direction of the void, reflecting the formation of an overdense boundary around the void.

The variety and extent of the tidal impact of voids on their environment can be appreciated from the other three panels in figure 15.

The top righthand panel is a telling illustration of their influence on the dynamics of filaments: the tidal bars trace the three filamentary structures that are connecting to the node at the top righthand corner of the panel. Evidently, the implication is that voids are instrumental in effecting further compression of the filaments. Overall, we see that the void induced tidal force field follows the underlying mass distribution in meticulous detail, which we find to be an exclusive property of the void population. Even on scales smaller than a few Mpc the voids are able to closely trace out the underlying matter distribution. The tidal fields of the other components do not display this level of detail.

6.2 Tidal Field Structure

For comparison between the tidal influence of the various cosmic web components, figure 16 shows the tidal amplitude maps for each individual component of the cosmic web. The top left panel shows the filament tidal field, the top right panel shows the void tidal field, the bottom right panel shows the wall tidal field and the bottom right panel shows the tidal field for nodes. The first global impression offered by these maps is that the differences are starker than for the corresponding force fields.

On large scales, the amplitude maps for the filaments and walls share a similar pattern, be it that the tides generated by filaments is substantially stronger than that for walls. The fact that they share a similar large scale spatial structure is an expression of the fact that these anisotropic features are intimately related aspects of the weblike network of which they are the principal constituent elements. A clear difference with the corresponding force amplitude maps (fig. 7) is that the tidal fields rapidly drop to a negligible level directly outside the filaments and walls, a direct reflection of the more localised nature of the tidal field. In terms of the relative amplitudes the filament induced tidal forces are still dominant (see fig. 17), in particular within the filament and wall network of the cosmic web, but far less so than in the gravitational force field. Within the interior of the filaments, the filament induced tides stand out as by far the strongest influence. Wall induced tides are marginally stronger inside walls, somewhat stronger than those induced by (nearby) filaments and voids (see fig. 18).

The filament tidal amplitude field delineates a large scale pattern of massive elongated filamentary structures. With the elongated shape of the filaments is an outstanding fundamental aspect of the filament tidal field, this goes along with a rather substantial level of inhomogeneity along the filaments, with high amplitude peaks marking the immediate high-density environment of massive clusters or the branching connections with other filaments in the weblike network. It is a direct reflection of the wide range of densities of filaments (see e.g. Cautun et al. 2014) and of the large density variations along the ridges of filaments in the cosmic web (see Cautun et al. 2014), which manifest themselves strongly in the more localised nature of the tidal field (as opposed to the more large-scale nature of the force field).

The wall tidal amplitude map shares the dominant large scale features seen in the filament map, but also includes several different and significant characteristics. While the same large scale structures in the wall tidal field can be seen, their contrast is substantially less than that seen in the filament induced tidal field. Also the tidal strength induced by the walls shows far less internal variation, yielding a more coherent tidal field within the outlined structures. This is a direct consequence of the mass density in walls being more uniform and spanning a much narrower range than that of the filament population (see e.g. Cautun et al. 2014). By far the most outstanding difference to the filament tidal field, in addition to the degree of coherence, is

the presence of far more small-scale structure filling up the space between the dominant large scale structures. Throughout the entire volume, it outlines a more intricate weblike network marked by the tidal footprint of small walls. Often they surround or connect with each other to form the boundaries of small void regions. In implies the multiscale nature of the cosmic web to be more readily visible in the wall induced tidal field than that in the overpowering filament tidal field, the latter more dominated by the major arteries of the cosmic web.

It is the void induced tidal field that reveals a surprisingly different pattern than that seen in the filament tidal amplitude map. In a sense it extrapolates the trend seen in the wall tidal amplitude maps of the dominant presence of small scale weblike structure. It yields a rich spatial pattern marked by small scale voidlike regions, with their boundaries connected into a pervasive network, yielding an ordered assembly of small-scale voids surrounded by wall-like boundaries. The pattern is also coherent and has a rather uniform amplitude, a direct reflection of the narrow density range of these cosmic underdensities (Cautun et al. 2014). It suggests that voids are largely responsible for defining and outlining the small-scale structure of the cosmic web, and appears to imply that voids play a crucial role in the formation, development and spatial organisation of the multiscale cosmic web.

By contrast, the node tidal field offers the least significant contribution to the tidal field. Even more so than in the case of the corresponding force field, the node induced tides define a spatial distribution that is highly localised in the immediate vicinity of the cluster nodes. The field does not contain a clearly defined structure, and has the appearance of a random set of tidal monopoles, with a field strength falling off like r^{-3} .

6.3 Tidal field strength: statistical analysis

For a quantitative judgement over the relative and absolute role of the induced tidal fields in the cosmic web, we turn to a similar assessment as in the case of the cosmic web force field, in terms of the probability functions for the total and relative tidal force field. Overall, we find a similar hierarchy in tidal force dominance as that in the case of the force field. However, filaments are far less dominant in the tidal field than in the force field. Walls, and in particular voids, have a considerably larger impact in setting the tides in the Universe. By contrast, nodes do not have any influence outside their immediate vicinity they, despite their high density contrast sometimes in excess of a thousand.

The top panel of figure 17 compares the pdf of the amplitude of the tides generated by the individual cosmic web components. The amplitude $|T|_{tot}^{CWM}$ is given in units of the average amplitude of the total field, $\sigma(|T|)$. The distribution of the amplitude of the induced tidal fields shows a substantial difference between the various components. Voids are by far the most ubiquitous components in the medium range of tidal values, in between $0.15 < |T|_{norm} < 0.5$. This is a clear reflection of their substantial tidal imprint, as we have already noticed in the amplitude maps, and the fact that they occupy a major fraction of the cosmic volume.

Walls and filaments have a major presence at low tidal amplitudes, with a mode near $T_{norm} \approx 0.1$, a reflection of the rapid falloff towards low tidal strengths outside of their own realm. However, both have a long tail towards high tidal values, ie. for $T_{norm} > 0.5$. It even leads to an average value substantially higher than that for voids, as may be seen in table 3. The filament tail reaches the highest tidal values, confirming the visual impression of figure 16, with the walls remaining at more moderate tidal values. The high tidal values

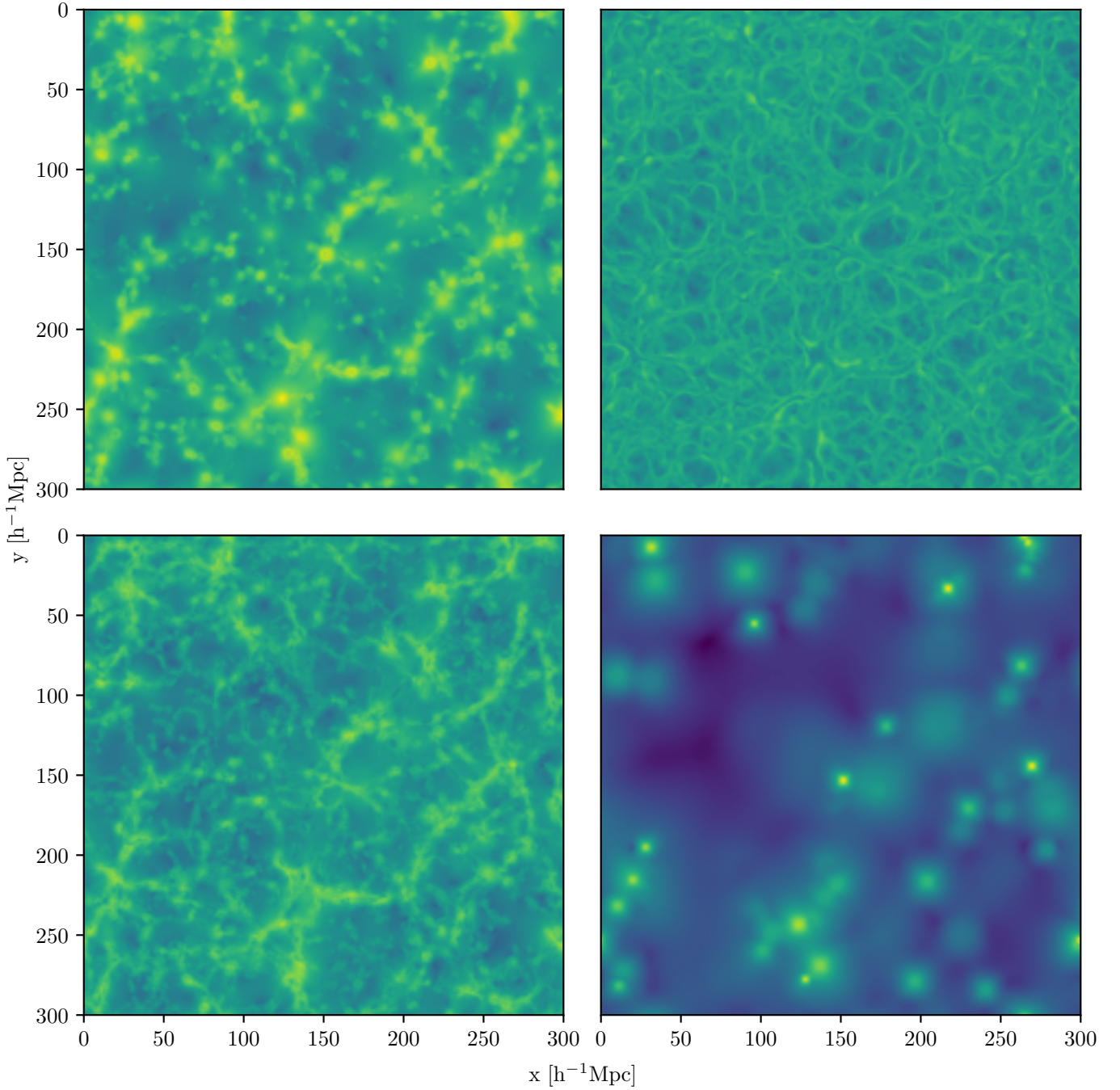


Figure 16. Tidal field by Cosmic Web component: amplitude field. The amplitude of the tidal field $\log_{10} |T|$ for the different components of the cosmic web for a $300 h^{-1} \text{Mpc}$ by $300 h^{-1} \text{Mpc}$ by $0.59 h^{-1} \text{Mpc}$ slice. The top left panel shows the component originating from filaments, the top right panel shows the component originating from voids, the bottom left panel shows the component originating from walls and the bottom right panel shows the component originating from nodes.

for these structures are a direct reflection and manifestation of the corresponding mass concentration in lower dimensionless geometric structures, i.e. of their elongated and flattened geometry. In turn, these are the result of their formation driven by the gravitational contraction induced by these anisotropic forces.

Telling is also the conclusion that quantitatively cluster nodes play only a minor role in setting the overall tidal force field. In most of the cosmic volume the nodes take care of only minor tidal values. The fact that their tidal pdf has a very long but low tail hints at their

dominance in the minute regions of their immediate neighbourhood, but nowhere else.

Upon assessing in which environments the various component tidal influences hold sway, we notice substantial differences in the case of voids and filaments, far less so for walls and cluster nodes. Overall, the wall and node contributions to the tidal inventory of the cosmic web appear to be far less dependent on location than that of

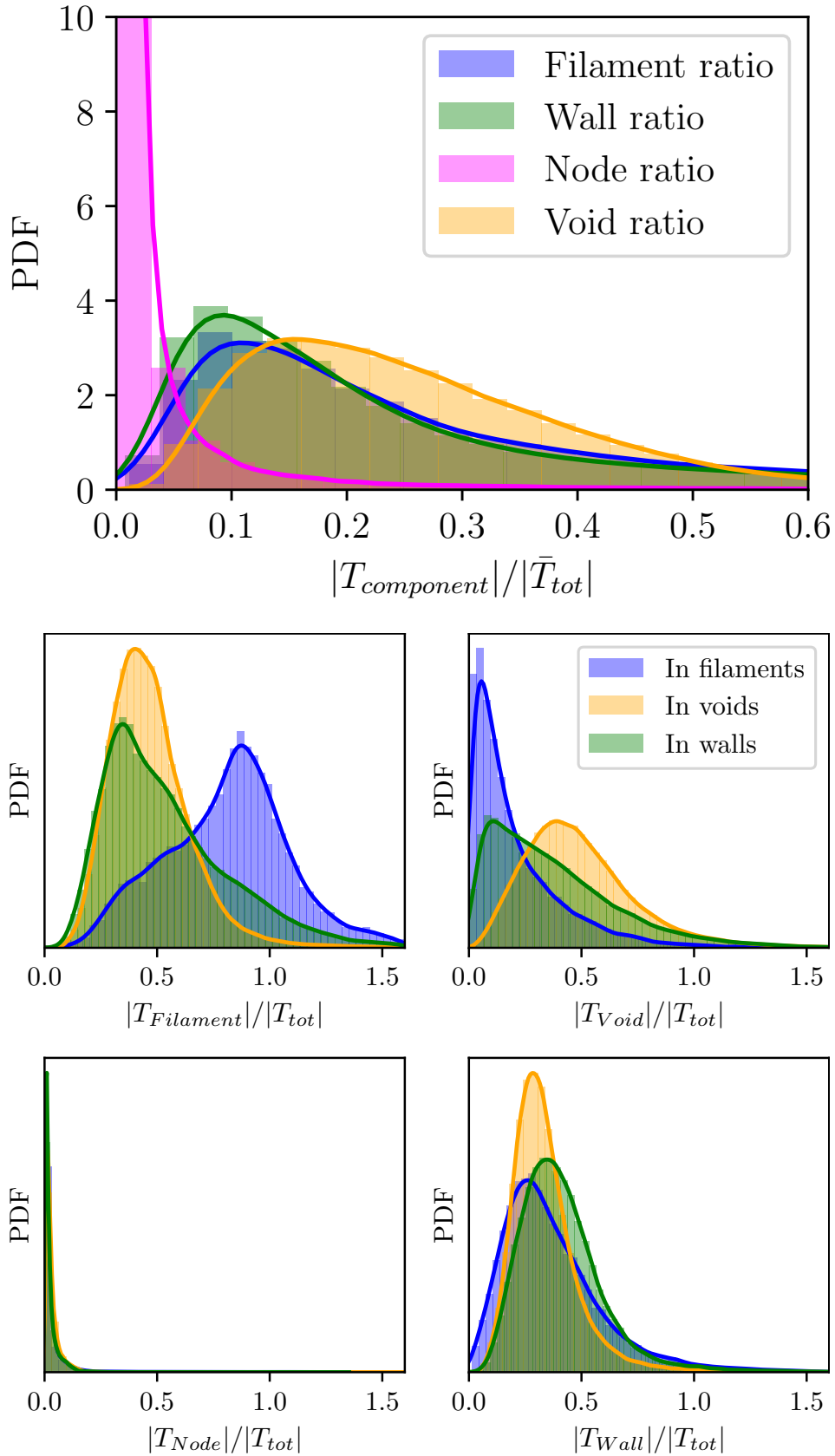


Figure 17. Cosmic Web Tidal Field: Strength Inventory. Top panel: The distribution of $|T|^{CWM}/|T_{tot}|$ for the different components of the cosmic web. This is the distribution for the entire field. Bottom four panels: the distribution of $|T|^{CWM}/|T_{tot}|$ for the different components of the cosmic web. Per panel the pdf for cosmic web component CWM is plotted, within three different environments: filaments (blue), voids (yellow), walls (green). Centre left: filament induced tidal field. Centre right: void induced tidal field. Bottom left: wall induced tidal field. Bottom right: cluster induced tidal field.

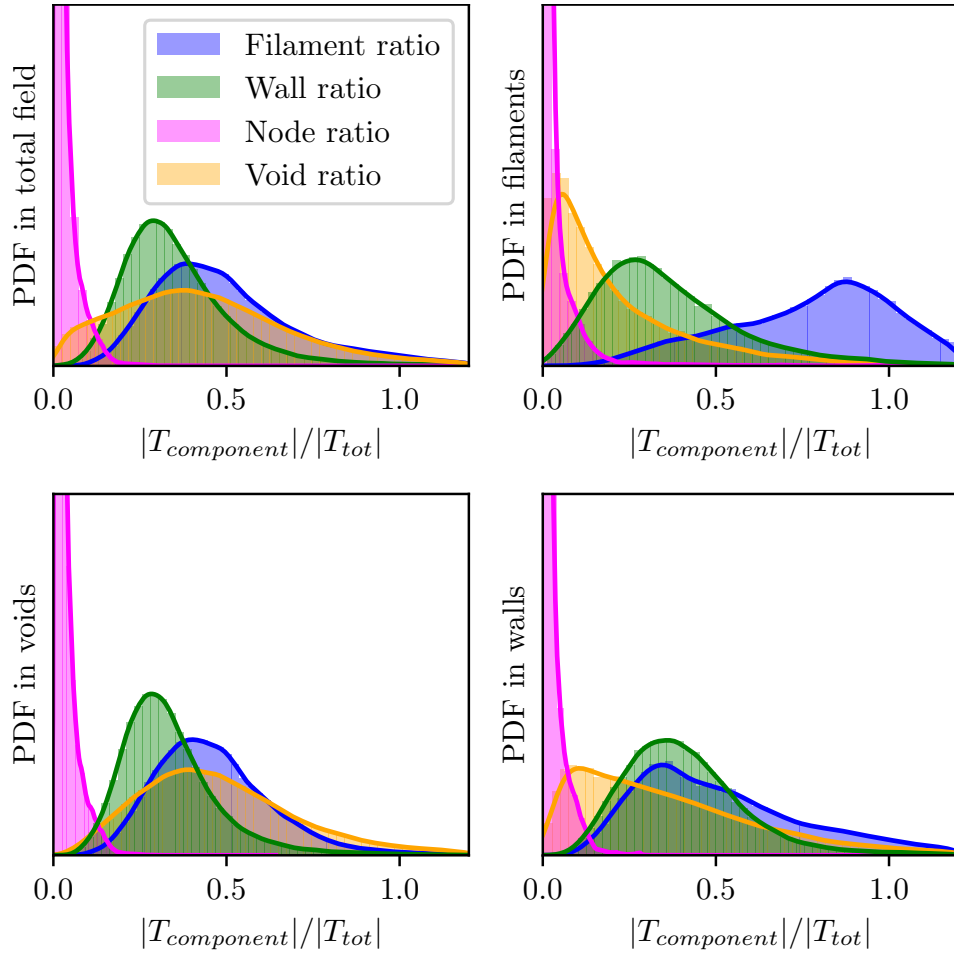


Figure 18. Cosmic Web Tidal Field: Strength Inventory by Cosmic Web environment. The panels show the pdf of the induced tidal field $|T|^{CWM}/|T|_{tot}$ by each of the four cosmic web components CWM in the different cosmic web environments. The different colours represent the different components: filament tidal field (blue), void induced tidal field (yellow), wall induced tidal field (green) and cluster node induced tidal field (magenta). Top left panel: total tidal field. Top right panel: tidal field in filaments. Bottom left panel: tidal field in voids. Bottom right panel: tidal field in walls.

Table 3. Tidal field statistics. The middle two columns show the mean tidal force ratio for the different components of the cosmic web using either global or local normalisation. Note the direction dependence in the ratio $|T|^{CWM}/|T|_{tot}$ and $|T|^{CWM}/|T|_{tot}$. The fourth column shows the percentage of the volume where each component is larger than all other components.

Component	Global [%]	Local [%]	Largest in [%]
Filaments	65.3	51.5	48.5
Voids	26.9	45.2	41.0
Nodes	3.5	3.0	0.1
Walls	34.9	36.2	10.4

filaments and voids. For the nodes this is largely because of their spatially severely limited influence.

Evidently, the relative filament and void influence are highly dependent on their location in the cosmic web. The four panels in figure 17 show the distribution of the relative filament, void, cluster and wall tidal contribution in either filaments (purple), void (orange) or wall (green) environments. The top righthand panel reveals the dominance of the filamentary induced tides within the realm of the filaments themselves, with the related panels for voids and walls indicating only a minor influence of these structures within filaments.

Meanwhile, the tidal influence of voids appears to be largely restricted to that in voids themselves. Walls hardly ever are a dominant tidal source, even not within walls themselves, although they always appear to represent an omnipresent minor influence.

The latter implies that the dynamics of filaments is largely propelled by the filamentary network itself. This is emphasised in the accompanying panels in figure 18, which for each of the cosmic web environments shows the distribution of the relative tidal impact by filaments, walls, voids and cluster nodes. Within filaments (top right-hand panel), tidal forces are mostly due to the influence of filaments themselves, with a moderate but substantially weaker influence by walls, and far less by voids and cluster nodes. The moderate influence by walls is an expression of the close spatial and geometric relation between the anisotropic filamentary and wall-like elements in the cosmic web.

Void regions show a more chequered tidal image. From the bottom lefthand panel of figure 18, we see that within voids, the tidal forces induced by the voids themselves represent a major influence, usually taking care of up to 40–50% of the tidal force field. Nonetheless, the impact of the surrounding filaments remains important and often is even dominant (the long tail of the pdf). To a lesser extent this is also true for the walls. This often concerns the outer parts and boundary regions of the voids, where the dynamical influence of the higher

density of filaments rapidly takes over the gravitational influence of the underdense voids. It emphasises the observation seen earlier with respect to the gravitational force field, the fact that the dynamics and dynamical evolution of voids cannot be understood without taking into account the external influence by in particular filaments.

6.4 Tidal field alignment

Given the notion that the elongated filamentary ridges and flattened walls in the cosmic web are the result of the tidally induced deformation of primordial matter concentrations, we should recognise this in the existence of an alignment of filaments and walls with respect to the tidal force field. To assess to what extent structures are aligned, we include a rough appraisal of the orientation of structures in the cosmic web with the tidal eigenvectors.

At each location we measure the alignment between the local geometry of the mass distribution and the tidal force. To this end we determine the orientation between the eigenvectors of the local tidal tensor and the eigenvectors of local inertia tensor. The latter is represented by the Hessian $\mathcal{H}(\mathbf{x})$ of the density field

$$H_{ij}(\mathbf{x}) = \frac{\partial^2 \Delta(\mathbf{x})}{\partial x_i \partial x_j}. \quad (23)$$

The eigenvectors of the Hessian are \hat{e}_1 , \hat{e}_2 and \hat{e}_3 , with corresponding eigenvalues

$$e_1 > e_2 > e_3 \quad (24)$$

$$|e| = \sqrt{e_1^2 + e_2^2 + e_3^2}. \quad (25)$$

A schematic diagram indicating the eigenvectors, of both tidal and inertia tensor, with respect to an elongated filament is shown in figure 19. Our alignment analysis investigates the orientation between the largest - compressional - tidal eigenvector, \hat{T}_1 and the inertia eigenvector along the ridge of the filament, ie. the smallest density Hessian, \hat{e}_3 . In a perfectly aligned setting, the compressional tidal eigenvector \hat{T}_1 would be expected to be perpendicular to the filament's ridge, and hence to \hat{e}_3 , implying an inproduct

$$\cos(\theta) = \hat{T}_1 \cdot \hat{e}_3 = 0. \quad (26)$$

On the other hand, in the absence of any correlation between the shape of the structure and the tidal field, the orientation θ between \hat{T}_1 and \hat{e}_3 would be random and the distribution of $\mu = \cos \theta$ entirely uniform (flat).

While the diagram in figure 19 relates to filaments, similar geometric considerations also hold for walls and voids. In the case of walls, \hat{e}_3 is one of the two eigenvectors directed along the plane of a wall, while \hat{T}_1 is the compressional tidal component, ideally directed perpendicular to the wall. For voids, the compressional tidal component \hat{T}_1 is expected to be directed along the radial direction of the void (see eqn. 22). To first approximation, inside voids the density hardly varies along radial shells, so that the density Hessian eigenvector \hat{e}_3 is oriented along the transverse direction of the void.

The distribution of the orientation angle $\cos(\theta)$ between \hat{T}_1 and \hat{e}_3 for the different cosmic web environments is shown in the four panels of figure 20. For the entire field, as well as for the void, filament and wall environments, the panels depict the orientation pdf for the compressional component of the complete tidal force \hat{T}_1 , as well as for the corresponding compressional components for each of the cosmic web components CWM, \hat{T}_1 .

All panels reveal a substantial level of alignment between the compressional tidal force and the local geometry of the environment.

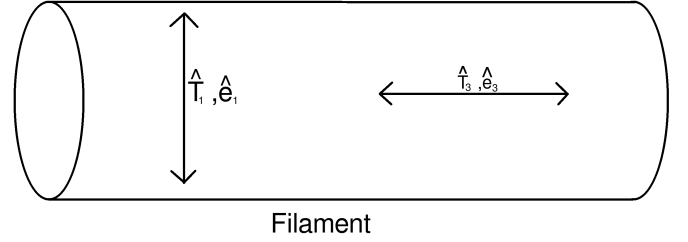


Figure 19. Tidal field & Cosmic Web alignment. Diagram illustration of (idealized) orientations inertial (Hessian density field) and tidal eigenvectors with respect to an elongated filament. Indicated is the orientation of the largest tidal eigenvector (T_1) and that of the smallest inertia eigenvector e_3 , which is aligned along the principal ridge of the filament.

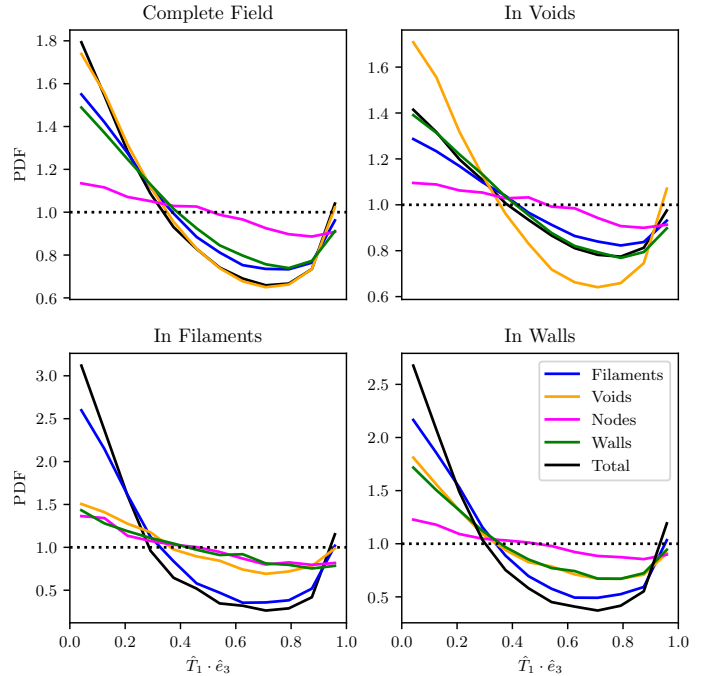


Figure 20. Tidal field & Cosmic Web alignment. The pdf of the alignment angle $\cos \theta = \hat{T}_1 \cdot \hat{e}_3$ between the largest (compressional) tidal eigenvector and the inertia tensor direction along the filament ridge, \hat{e}_3 . The four panels show the pdf curves for the tidal field induced by the entire mass distribution and the specific tidal fields induced by the four morphological components CWM in four different cosmic web environments. Black curve: tidal field induced by entire mass distribution; blue curve: filament induced tidal field; orange curve: void induced tidal field; green curve: wall induced tidal field; magenta curve: cluster node tidal field. The environments in the four panels: entire field (top lefthand panel); void regions (top righthand panel); filament regions (bottom lefthand panel); wall region (bottom righthand panel). Note the different range for the vertical axis of the four panels.

The distribution functions peak strongly towards $\mu = \cos(\theta) = 0$, ie. we find a strongly perpendicular tendency. The one major exception is that for the node induced tidal force, which in all environments shows a mere weak alignment. It is a manifestation of the weak cluster node induced tidal field throughout the entire volume. With respect to filaments and voids the following observations are made:

- Filaments

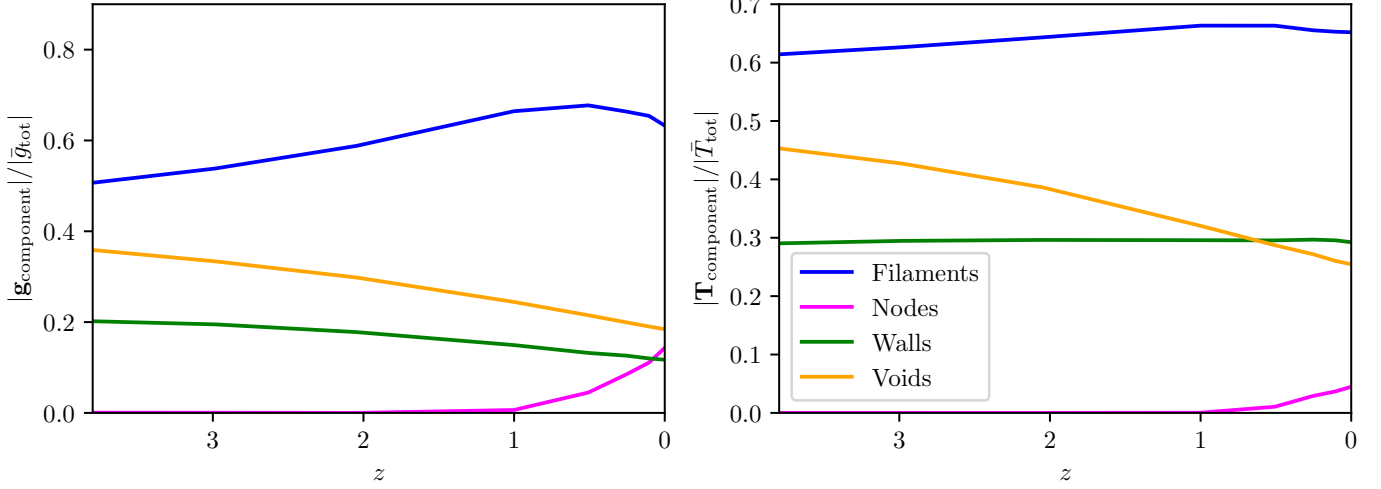


Figure 21. Redshift Evolution Forces and Strains in the Cosmic Web. Left frame: redshift evolution of the global average gravitational force fraction $\mathcal{F}^{\text{CWM}} = |g|^{\text{CWM}}/|g|^{\text{total}}$ for the force induced by cosmic web component CWM. Right frame: redshift evolution of the global average tidal field fraction $\mathcal{F}^{\text{CWM}} = |T|^{\text{CWM}}/|T|^{\text{total}}$ for the tide induced by cosmic web component CWM.

Inside filaments, the alignment between tide and geometry can be almost exclusively ascribed to the the filament induced tidal force. To a lesser extent, the filament induced tide is responsible for a major share of alignment in walls, confirming yet again the strong structural bond between filaments and walls. Hence, the filament induced tides are not only dominant with respect to their amplitude and strength, but also with respect to their orientation and dynamical impact. On the other hand, we also see that even within filamentary environments, the filament induced tides do not account for all alignments. It hints at the still significant influence by the other cosmic web components, in particular voids and walls.

- Voids

A most interesting finding is that the mass distribution inside voids is more strongly aligned with the tidal field than that in the overall field (top righthand frame fig:tidangd). To a large extent this is to be ascribed to the strong alignment with the tidal force induced by the void itself. Also, we find that the latter has only a weak alignment with the ridge of filaments (bottom righthand frame fig. 20), and a mere moderate alignment with the plane of walls (top righthand frame fig:tidangd). In all, it confirms the earlier impression of the voids tidally dominating the more tenuous parts of the cosmic web.

7 COSMIC WEB FORCE & TIDAL EVOLUTION

The present study has concentrated predominantly on the dynamical structure of the cosmic web at the current cosmic epoch, $z = 0$. In order to develop more definitive conclusions on the buildup of structure by the force and tidal influence of the various cosmic web components, it will be imperative not only to study the dynamics at the current time, but also to investigate their behaviour over time. While in an upcoming study we address the dynamical evolution of the cosmic web in detail, we may get a global impression by evaluating global averages of the force and tidal amplitudes as a function of redshift z .

We follow the evolution of the mean (normalized) force and tide contribution by the various cosmic web components - filaments, walls, voids and cluster nodes. To this end, for each redshift z , at each location \mathbf{x} we determine the fractional contribution $\mathcal{F}^{\text{CWM}}(\mathbf{x}, z)$ by

a component CWM to the total force or tide amplitude $\mathcal{A}^{\text{total}}(\mathbf{x}, z)$,

$$\mathcal{F}^{\text{CWM}}(\mathbf{x}, z) = \frac{\mathcal{A}^{\text{CWM}}(\mathbf{x}, z)}{\mathcal{A}^{\text{total}}(\mathbf{x}, z)}. \quad (27)$$

By normalizing with respect to the average (total) force or tide amplitude at redshift z , we compensate for the time evolution of the general force and tidal fields. We average over all locations \mathbf{x} to obtain a global fractional average $\tilde{\mathcal{F}}(z)$ at redshift z .

Figure 21 plots the redshift evolution of the fractional force contributions by cosmic web components CWM (lefthand panel) and corresponding fractional tidal amplitude contributions (righthand panel), over a redshift range $0 < z < 4$. On the basis of these rudimentary global averages, a few generic conclusions may be drawn with respect to the evolution of cosmic web dynamics.

Over the entire redshift range, filaments are consistently by far the most dominant cosmic web component, with respect to both force and tidal fields. Up to a redshift $z \approx 0.5 - 1$, the influence of filaments is increasing, partially the reflection of the growth of the filament population and mass as cosmic structure develops (see e.g. Cautun et al. 2014). The influence of filaments stabilises after this redshift, and may even decrease somewhat. It is tantalising to identify this with the universe transiting from a matter-dominated to a dark energy dominated regime, and the corresponding global stemming of structure growth as the Universe enters an exponential de Sitter expansion phase. Another factor may be that of the steep emergence and growth of massive cluster nodes, whose fractional force and tidal influence we see rising steeply after $z \approx 1$ (see fig. 21, magenta curve). This goes along with the accretion of large amounts of mass along dense filamentary branches connecting the filamentary arteries with the cluster nodes, and the subsequent increasing force influence of the nodes. At high redshifts the influence of cluster nodes is almost negligible, as their hierarchical buildup has not yet formed virialized clusters of comparable mass.

Arguably the most interesting evolutionary trend is seen for the void population. The force and tidal field influence of voids turns out to be even more prominent at higher redshifts than it is today. To some extent this may seem surprising. Because voids are smaller and less empty at higher redshifts, at first one might expect them to have a weaker influence over the cosmic mass distribution. On the

other hand, the filamentary and wall-like skeleton of the cosmic web is also developing rapidly at high redshifts, and represents less mass at those redshifts. Relatively speaking, voids may therefore be more prominent at high redshifts. The details of the dynamical influence of voids, of the induced mass migration out of their interior, within the context of the hierarchically evolving void populations (Sheth & van de Weygaert 2004; Aragon-Calvo & Szalay 2013), therefore need further investigation. This is the subject of a related upcoming study.

Finally, walls offer a chequered view of force and tidal evolution. Their tidal influence appears to remain almost constant throughout time. Their force evolution, however, appears to follow a similar downward trend as that seen for the void population. It may reflect a proportionally higher mass content at higher redshift, a consequence of the flow of mass from void troughs, via walls towards filaments.

8 SUMMARY AND DISCUSSION

The cosmic web emerges at the transition between the linearly evolving cosmic matter distribution on large cosmological scales, and the highly nonlinear realm on small scales where we find matter assembled in virialized halos (Bond et al. 1996; van de Weygaert & Bond 2008a; Cautun et al. 2014; Libeskind et al. 2018). At this transition scale, we see the emergence of complex spatial structure in the shape of an intricate weblike pattern. Long elongated filaments and flattened tenuous planar walls form the boundaries of near-empty void regions and defined a pervasive interconnected network, whose dense compact nodes are the sites where we find massive virialized halos.

With the cosmic web forming the manifestation of this key dynamical transition in the organisation of the cosmic matter distribution, it is essential to develop a more profound insight and understanding of the dynamics driving the buildup of cosmic structure, of the induced migration flows, and the gravitational influence of the various constituents of the cosmic web on these processes. This will bear upon a range of major cosmological issues. Prime is a more fundamental understanding of the formation and assembly of the cosmic web itself, and its relation to the primordial mass distribution (see e.g. Feldbrugge et al. 2018b; Feldbrugge & van de Weygaert 2024). Of major current interest is the influence of the large scale environment on the formation and evolution of galaxies, of which the most widely recognised factor is that of the generation of angular momentum of galaxies by tidal torquing by the same tidal forces that shape the filaments and walls in the cosmic web (e.g. Hoyle 1949; White 1984; Porciani et al. 2002a,b; Jones & van de Weygaert 2009; Codis et al. 2012, 2015; Ganeshiaiah Veena et al. 2019). Of increasing interest is also the potential information content of the intricate cosmic web structure on the value of cosmological parameters and the properties of dark matter and dark energy. Over the recent years in particular the structure and kinematics of cosmic voids have received ample attention for the potentially high precision with which they may reflect the character and value of dark energy (see e.g. Lee & Park 2009; van de Weygaert & Platen 2011; Lavaux & Wandelt 2012; Bos et al. 2012; van de Weygaert 2016; Pisani et al. 2019).

The present study is the first stage in a systematic investigation of the detailed dynamics involved in the emergence and assembly of the cosmic web and its various morphological components. We assess the force field and tidal field induced by filaments, walls, cluster nodes and voids, and investigate in how far they contribute, and dominate, the gravity and tides in the various regions of the cosmic

web. It facilitates an in-depth investigation of the role of the different morphological components of the cosmic web, and its environmental dependence, in driving the gravitational evolution driven formation and evolution of the largest structures in the universe.

The dynamical inventory study is based on the redshift $z = 0$ structure in a 512^3 large Λ CDM dark matter only N-body simulation in a $(300h^{-1}\text{Mpc})$ box. At each location in the simulation box the gravitational force and tidal tensor is computed for the entire mass content in the simulation volume, as well as separate for the force and tides generated by filament regions, walls, void regions and cluster nodes separately. In the current study this is based on a brute-force direct summation over the mass elements residing in the various identified morphological structures. Given the morphological identity of each mass element, we are able to do the gravitational force and tidal field analysis separately for the various cosmic web regions. Hence, it allows us to study in how far the dynamics of voids is influenced by the surrounding filaments or, reversely, in how far the gravitational force and tidal forces in filaments are feeling the presence of the surrounding voids. In addition, it enables an evaluation of the reach of void induced forces and tides, the scales over which filaments dominate, and a wide range of related issues.

For the identification of the cosmic web structures, we invoke the density field NEXUS+ multiscale morphological formalism (Aragón-Calvo et al. 2007b,a, 2010; Cautun et al. 2013, 2014), which delineate the filament, void, wall and node regions. NEXUS+ is the highest dynamic range version of the Scale Space MMF/Nexus pipeline, unique in its combination of geometric and dynamical criteria for the morphological classification and that of taking into account of the multiscale nature of the cosmic matter distribution. It enables us to identify structures over a wide spectrum of scales and densities, and hence assures an optimal assessment of the multiscale aspects of cosmic web dynamics. The NEXUS formalism assigns to each location in the simulation volume the appropriate morphology - filaments, walls, void or cluster node - following a parameter-free evaluation at the proper physical scale of the locally dominant feature.

The systematic inventory of cosmic web dynamics yielded insights that confirm existing assumptions. More tantalising are new and surprising insights with respect to the role of voids and cluster nodes. Amongst the conclusions based on the presented force and tide inventory are:

- The gravitational force fields generated by the distinct cosmic web components differ significantly from each other. The gravitational fields induced by filaments, voids, walls and cluster nodes have markedly and systematically dissimilar characters. The overall amplitude of the gravitational force, their range, and spatial structure and pattern are quite dissimilar. In terms of the amplitude of the induced forces, there is a clear hierarchy: filaments are by far the most dominant and powerful force, followed by voids, only then - surprisingly - by cluster nodes, followed by walls.

- At nearly every location, the total gravitational force is the combination of the contributions by several cosmic web components. The important implication is that it is hardly possible to describe the dynamics and development of a structure as an isolated object. In general the gravitational influence is the result of the interplay between the several contributions. The only exceptions may be the force field in the interior of the most prominent filaments and in and around the immediate vicinity of massive cluster nodes. Yet, over most of the filamentary network also the influence of nearby voids should be taken into account, while the dynamical evolution of walls cannot be understood at all without taking into account the impact

by the nearby filaments and voids. It certainly is true without any exception for all void regions, whose dynamics cannot be understood on the basis of their underdense interior but should also take into account the even more dominant exterior influence by the nearby filaments.

- Filaments dominate the gravitational force field over nearly the entire cosmic volume, with the exception of the immediate vicinity of the massive cluster nodes. On average, they are responsible for more than 50% of the exerted gravitational force at any location. Filaments' exert their influence over a large spatial range.

- While voids turn out to represent a sizeable gravitational influence over nearly the entire cosmic volume, they hardly dominate anywhere, even within their own interior. Instead, at a large fraction of space they are the second gravitational influence after filaments.

- Voids have a limited spatial range over which they wield their gravitational influence. The spatial pattern defined by the void generated gravitational field is one of a segmented volume, each segment surrounding a locally strong repulsive density trough (with radii up to $50 h^{-1} \text{Mpc}$. Zooming in on individual void regions shows their superhubble expanding effect over their interior and up to their overdense boundary. Within the interstitial regions between voids, i.e. for their filamentary and planar boundaries, their gravitational impact declines rapidly to very low levels.

- Despite the mostly segmented nature of the void induced force field, still we find a residual large scale void force field. This is a manifestation of the multiscale nature of the void population (see [Sheth & van de Weygaert 2004](#); [Aragon-Calvo & Szalay 2013](#)), a direct result of its hierarchical evolution and which has recently been detected in the observational Cosmicflows-3 peculiar velocity field ([Courtois et al. 2023](#)).

- A complete dynamical description of voids in terms of isolated expanding underdense regions is not representative. The evolution of voids depends strongly on the exterior mass distribution. Void dynamics is predominantly a combined effect of the induced superhubble expansion by voids themselves and the force and tidal influence of the surrounding filaments (and, if in their near vicinity, the nearby cluster nodes). It shows that any consideration of void dynamics in terms of isolated almost spherically expanding regions needs a fundamental revision: the dynamics of voids cannot be understood without taking into account the gravitational and tidal influence of the environment.

- A surprising finding is that of the rather low dynamical influence by massive cluster nodes. Both the gravitational force induced by cluster nodes, as well as the corresponding tidal force, are only significant in and in the immediate surroundings of the cluster nodes, out to a radius of $\approx 5 h^{-1} \text{Mpc}$. Because of their rather limited gravitational influence, they only wield a minor impact on the structure of the cosmic web.

- With respect to the corresponding gravitational tides, the situation in terms of strength is less outspoken than in the case of the gravitational force. Still, filaments are the strongest source of gravitational tides. However, voids, and even walls, yield a significant additional and alternative tidal influence. While the tidal impact of filaments has a predominantly large scale character, strongly correlated with the main elongated arteries in the cosmic web, walls and in particular voids add an essential small-scale aspect of the tidal field that is to be identified with the multiscale nature and structure of the cosmic web.

- The tidal field generated by filaments is largely a large-scale phenomenon, reflecting the outline of the most massive and promi-

nent arteries in the cosmic web. The multiscale structure of the cosmic web can hardly be recognised in the filament induced tidal field. Filaments are the predominant source for the tidal forces inside the filaments themselves, as a result of their overwhelming strength within the filamentary ridges of the cosmic web.

- Along the filamentary ridges, the tidal field generated by filaments is rather inhomogeneous and patchy, marked by a fluctuating trend between high amplitude and low amplitude regions along a filament's ridge. This is a direct manifestation of the rather strong mass density variations along a filament's ridge (see e.g. [Cautun et al. 2014](#)). With respect to the orientation of the tidal force field along filaments, we see a coherent pattern of aligned compressional tidal bars along the ridge of a filament.

- Voids are the dominant source of tidal influence within their interior. As voids represent the major share of a cosmic volume, void assume a major organising role in the shaping of the cosmic matter distribution.

- An interesting finding is the remarkable spatial pattern in the void induced tidal amplitude map: the void tidal field defines a coherent rather uniform cellular pattern over the entire volume, dominated by the small-scale voids in the multiscale buildup of the cosmic web. The void tidal field appears to trace the cosmic web down to even the most tenuous structures found inside voids (also see [Aragon-Calvo & Szalay 2013](#), with respect to a similar observation wrt. the interior void velocity field).

- The finding that the spatial organisation of the cosmic web is most readily expressed in the void tidal field suggests voids to be seen as the organisers of the cosmic web. It is confirmed by the orientation of the void induced tidal field (see the case studies in [fig. 15](#)): the compressional component appears to trace the more tenuous parts of the cosmic web, suggesting them to be responsible for the shaping of the tenuous walls and filaments that form the boundaries of the small voids. Analysis of the alignment between tidal field and mass distribution underlines this conclusion, revealing a stronger alignment within the interior of voids than in the overall cosmic web.

- The tidal force field induced by the wall population is more noticeable than its gravitational force field, arguably the reflection of their intimate relationship with the filamentary spine of the cosmic web. Both are the product of the anisotropic force field emanating from the inhomogeneous mass distribution, i.e. from the tidal force field. The wall tidal field follows the large scale spatial outline seen in the filament tidal field, tracing the heavy arteries and connecting sheets in the cosmic web. Yet, it also reflects - more faintly - the small-scale cellular pattern seen in the void induced tidal field.

While most of our analysis concerns the current cosmic matter distribution, a global statistical overview shows that the overall conclusions concerning strength of the gravitational force and tidal forces generated by the various cosmic web components pertains over a rather wide range of redshifts, at least from $z = 4$ down to $z = 0$.

In summary, we find that filaments are the main drivers of the dynamical evolution of the cosmic web. This may not be surprising, given filaments represent at least $\approx 50\%$ of the mass in the universe, concentrated in rather compact elongated ridges pervading the entire universe. More revealing is the finding of the prominent role of voids in the dynamics of the cosmic web. When looking at the cause of anisotropic structure, of which tidal fields are the main agent, we find that voids play an important role. In other words, they can be seen as the main spatial organisers of the multiscale cosmic web.

This work has the intention to open the window on to the intricate

interplay of the various gravitational influences in the cosmic web. It is the starting point of a more extensive program. Several immediate and evident practical and computational improvements of the current study are foreseen. These include a more efficient force and tidal tensor computation that would enable a more detailed statistical study and the extension of our study to large cosmological simulations including gas dynamics, baryonic physics and galaxy formation. More fundamental will be the astrophysical and cosmological issues that should be addressed on the basis of the new insights gained from the present inventory of cosmic web dynamics. Amongst a wide range of related issues, two prominent aspects are the following.

The most outstanding issue to be addressed is that of the dynamics and evolution of cosmic voids. In a follow-up study the multiscale structure of the void force and tidal field, as well as the generated mass flows, will be analysed armed with the insights obtained in the current study. The low-density environment in voids imply the major influence of external gravitational and tidal influences. As demonstrated in the present study, for most void configurations it is essential to include the role of the surrounding filamentary cosmic web if we seek to understand and exploit their structure and flow fields. This will alter our understanding of galaxy formation and evolution within void environments, given for example the impact on matter accretion. It will substantially impact on the use of voids as cosmological probes, given the fact that their internal structure and dynamics will even more highly altered by the surrounding cosmic web structure than by cosmological factors.

Another important observable effect of the cosmic web is that on the shape and rotation of galaxies. While it has long been recognised that especially the strong tidal forces exerted by (proto)filaments are the principal source of rotation for many galaxies, many recent studies have uncovered additional processes such as the anisotropic accretion along filaments that may seriously affect the outcome. In a slightly different context, the tidal forces induced by the cosmic web yield intrinsic alignments of gravitationally lensed background galaxy images and their interpretation within the cosmological context. Given the current study's finding that the tidal force field is highly sensitive to the small-scale aspects of the cosmic web, highlighting the presence of small voids and walls that are observationally difficult to detect, it may be necessary to focus in more detail on the intricate dynamical structure of the cosmic web and its effect on to compensate for its impact.

ACKNOWLEDGEMENTS

We are grateful to Marius Cautun and Bernard Jones for their willingness to share the Nexus code for this project, and to Joop Schaye for helpful suggestions. Many decades ago Vincent Icke taught RvdW about the importance of voids, the present study is a token of gratitude for this wise lesson. RvdW owes Dick Bond for emphasizing the key role of tidal forces to understand the formation of the cosmic web. Finally, RvdW also acknowledges Simon White for a highly motivating remark that inspired a major share of the current study. This work is partly funded by research programme Athena 184.034.002 from the Dutch Research Council (NWO).

DATA AVAILABILITY

All data presented in this paper will be shared upon reasonable request to the corresponding author.

REFERENCES

- Abel T., Hahn O., Kaehler R., 2012, *MNRAS*, **427**, 61
 Alam S., Paranjape A., Peacock J. A., 2024, *MNRAS*, **527**, 3771
 Alpaslan M., et al., 2014, *MNRAS*, **438**, 177
 Angulo R. E., Zennaro M., Contreras S., Aricó G., Pellejero-Ibañez M., Stücker J., 2021, *MNRAS*, **507**, 5869
 Aragon-Calvo M. A., Szalay A. S., 2013, *MNRAS*, **428**, 3409
 Aragon-Calvo M. A., Yang L. F., 2014, *MNRAS*, **440**, L46
 Aragón-Calvo M. A., Jones B. J. T., van de Weygaert R., van der Hulst J. M., 2007a, *A&A*, **474**, 315
 Aragón-Calvo M. A., van de Weygaert R., Jones B. J. T., van der Hulst J. M., 2007b, *ApJ*, **655**, L5
 Aragón-Calvo M. A., van de Weygaert R., Jones B. J. T., 2010, *MNRAS*, **408**, 2163
 Awad P., et al., 2023, *MNRAS*, **520**, 4517
 Bernardeau F., van de Weygaert R., Hivon E., Bouchet F. R., 1997, *MNRAS*, **290**, 566
 Bocquet S., Heitmann K., Habib S., Lawrence E., Uram T., Frontiere N., Pope A., Finkel H., 2020, *ApJ*, **901**, 5
 Bond J. R., Kofman L., Pogosyan D., 1996, *Nature*, **380**, 603
 Bonjean V., Aghanim N., Salomé P., Douspis M., Beelen A., 2018, *A&A*, **609**, A49
 Bos E., 2016, PhD thesis, University of Groningen
 Bos E. G. P., van de Weygaert R., Dolag K., Pettorino V., 2012, *MNRAS*, **426**, 440
 Cautun M. C., van de Weygaert R., 2011, The DTFE public software: The Delaunay Tessellation Field Estimator code
 Cautun M., van de Weygaert R., Jones B. J. T., 2013, *MNRAS*, **429**, 1286
 Cautun M., van de Weygaert R., Jones B. J. T., Frenk C. S., 2014, *MNRAS*, **441**, 2923
 Cen R., 1997, *ApJ*, **479**, L85
 Codis S., Pichon C., Devriendt J., Slyz A., Pogosyan D., Dubois Y., Sousbie T., 2012, *MNRAS*, **427**, 3320
 Codis S., Pichon C., Pogosyan D., 2015, *MNRAS*, **452**, 3369
 Colless M., et al., 2003, *arXiv e-prints*, pp astro-ph/0306581
 Courtois H. M., et al., 2023, *A&A*, **673**, A38
 Dietrich J. P., Werner N., Clowe D., Finoguenov A., Kitching T., Miller L., Simionescu A., 2012, *Nature*, **487**, 202
 Efsthathiou G., Jones B. J. T., 1980, *Comments on Astrophysics*, **8**, 169
 Einasto J., 1977, in *Problems of Observational and Theoretical Astronomy*, pp 26–43
 Elek O., Burchett J. N., Prochaska J. X., Forbes A. G., 2020, *arXiv e-prints*, p. arXiv:2009.02441
 Elek O., Burchett J. N., Prochaska J. X., Forbes A. G., 2022, *arXiv e-prints*, p. arXiv:2204.01256
 Feldbrugge J., van de Weygaert R., 2023, *J. Cosmology Astropart. Phys.*, **2023**, 058
 Feldbrugge J., van de Weygaert R., 2024, *arXiv e-prints*, p. arXiv:2405.20475
 Feldbrugge J., van de Weygaert R., Hidding J., Feldbrugge J., 2018b, *J. Cosmology Astropart. Phys.*, **2018**, 027
 Feldbrugge J., van de Weygaert R., Hidding J., Feldbrugge J., 2018a, *J. Cosmology Astropart. Phys.*, **2018**, 027
 Feldbrugge J., Yan Y., van de Weygaert R., 2023, *MNRAS*, **526**, 5031
 Florack L., ter Haar Romeny B., Koenderink J., Viergever M., 1992, *Image and Vision Computing*, **10**, 376
 Forero-Romero J. E., Hoffman Y., Gottlöber S., Klypin A., Yepes G., 2009, *MNRAS*, **396**, 1815
 Frieman J. A., Turner M. S., Huterer D., 2008, *ARA&A*, **46**, 385
 Ganeshaiah Veena P., Cautun M., van de Weygaert R., Tempel E., Jones B. J. T., Rieder S., Frenk C. S., 2018, *MNRAS*, **481**, 414
 Ganeshaiah Veena P., Cautun M., Tempel E., van de Weygaert R., Frenk C. S., 2019, *MNRAS*, **487**, 1607
 Ganeshaiah Veena P., Cautun M., van de Weygaert R., Tempel E., Frenk C. S., 2021, *MNRAS*, **503**, 2280
 Hahn O., Carollo C. M., Porciani C., Dekel A., 2007, *MNRAS*, **381**, 41
 Hahn O., Teyssier R., Carollo C. M., 2010, *MNRAS*, **405**, 274
 Hidding J., van de Weygaert R., Vegter G., Jones B. J. T., Teillaud M., 2012,

- arXiv e-prints, p. [arXiv:1205.1669](https://arxiv.org/abs/1205.1669)
- Hidding J., van de Weygaert R., Shandarin S., 2016, in van de Weygaert R., Shandarin S., Saar E., Einasto J., eds, IAU Symposium Vol. 308, The Zeldovich Universe: Genesis and Growth of the Cosmic Web. pp 69–76 ([arXiv:1611.01221](https://arxiv.org/abs/1611.01221)), doi:10.1017/S1743921316009650
- Hirschmann M., Dolag K., Saro A., Bachmann L., Borgani S., Burkert A., 2014, *MNRAS*, **442**, 2304
- Hoffman Y., Metuki O., Yepes G., Gottlöber S., Forero-Romero J. E., Libeskind N. I., Knebe A., 2012, *MNRAS*, **425**, 2049
- Hoyle F., 1949, eds. Burgers, J.M. and van de Hulst, H.C. (Central Air Documents Office, Dayton)
- Huchra J. P., et al., 2012, *The Astrophysical Journal Supplement Series*, 199, 26
- Hunter J. D., 2007, *Computing in Science & Engineering*, 9, 90
- Icke V., 1984, *MNRAS*, **206**, 1P
- Jones B., van de Weygaert R., 2009, *Astrophysics and Space Science Proceedings*, **8**, 467
- Jones B. J. T., van de Weygaert R., Aragón-Calvo M. A., 2010, *MNRAS*, **408**, 897
- Kitaura F.-S., Angulo R. E., Hoffman Y., Gottlöber S., 2012a, *MNRAS*, **425**, 2422
- Kitaura F.-S., Erdoğdu P., Nuza S. E., Khalatyan A., Angulo R. E., Hoffman Y., Gottlöber S., 2012b, *MNRAS*, **427**, L35
- Kourkchi E., et al., 2020, *ApJ*, **902**, 145
- Lavaux G., Wandelt B. D., 2012, *ApJ*, **754**, 109
- Lee J., Park D., 2009, *ApJ*, **696**, L10
- Lee J., Pen U.-L., 2000, *ApJ*, **532**, L5
- Lee J., Springel V., 2010, *J. Cosmology Astropart. Phys.*, 2010, 031
- Lee J., Hahn O., Porciani C., 2009, *ApJ*, **705**, 1469
- Lee K. G., et al., 2018, VizieR Online Data Catalog, p. [J/ApJS/237/31](https://vizier.cfa.harvard.edu/votable/?outfmt=html&source=J/ApJS/237/31)
- Libeskind N. I., et al., 2018, *MNRAS*, **473**, 1195
- Lindeberg T., 1994, *Journal of Applied Statistics*, **21**, 225
- Liske J., et al., 2015, *MNRAS*, **452**, 2087
- López P., Cautun M., Paz D., Merchán M., van de Weygaert R., 2021, *MNRAS*, **502**, 5528
- Macquart J. P., et al., 2020, *Nature*, **581**, 391
- McCarthy I. G., Schaye J., Bird S., Le Brun A. M. C., 2017, *MNRAS*, **465**, 2936
- Meiksin A. A., 2009, *Reviews of Modern Physics*, **81**, 1405
- Neyrinck M. C., Shandarin S. F., 2012, [arXiv e-prints](https://arxiv.org/abs/1207.4501), p. [arXiv:1207.4501](https://arxiv.org/abs/1207.4501)
- Nicastro F., et al., 2018, *Nature*, **558**, 406
- Ostriker J. P., Cen R., 1996, *ApJ*, **464**, 27
- Paranjape A., 2021, *MNRAS*, **502**, 5210
- Park D., Lee J., 2007, *Phys. Rev. Lett.*, **98**, 081301
- Peebles P. J. E., 1969, *ApJ*, **155**, 393
- Peebles P. J. E., 1980, The large-scale structure of the universe
- Pichon C., Bernardeau F., 1999, *A&A*, **343**, 663
- Pillepich A., et al., 2018, *MNRAS*, **473**, 4077
- Pisani A., et al., 2019, *BAAS*, **51**, 40
- Platen E., van de Weygaert R., Jones B. J. T., 2008, *MNRAS*, **387**, 128
- Porciani C., Dekel A., Hoffman Y., 2002a, *MNRAS*, **332**, 325
- Porciani C., Dekel A., Hoffman Y., 2002b, *MNRAS*, **332**, 339
- Romano-Díaz E., van de Weygaert R., 2007, *MNRAS*, **382**, 2
- Schaap W. E., van de Weygaert R., 2000, *A&A*, **363**, L29
- Schäfer B. M., 2009, *International Journal of Modern Physics D*, **18**, 173
- Schaye J., et al., 2015, *MNRAS*, **446**, 521
- Schaye J., et al., 2023, [arXiv e-prints](https://arxiv.org/abs/2306.04024), p. [arXiv:2306.04024](https://arxiv.org/abs/2306.04024)
- Schlaflly E. F., et al., 2023, [arXiv e-prints](https://arxiv.org/abs/2306.06309), p. [arXiv:2306.06309](https://arxiv.org/abs/2306.06309)
- Shandarin S. F., 2011, *J. Cosmology Astropart. Phys.*, 2011, 015
- Shandarin S. F., Zeldovich Y. B., 1989, *Reviews of Modern Physics*, **61**, 185
- Shandarin S., Habib S., Heitmann K., 2012, *Phys. Rev. D*, **85**, 083005
- Sheth R. K., van de Weygaert R., 2004, *MNRAS*, **350**, 517
- Shim J., Codis S., Pichon C., Pogosyan D., Cadiou C., 2021, *MNRAS*, **502**, 3885
- Shivashankar N., Pranav P., Natarajan V., van de Weygaert R., Bos E. G. P., Rieder S., 2016, *IEEE Transactions on Visualizations and Computer Graphics*. Vol. 22(6), 22, 1745
- Sousbie T., 2011, *MNRAS*, **414**, 350
- Sousbie T., Pichon C., Kawahara H., 2011, *MNRAS*, **414**, 384
- Springel V., 2005, *MNRAS*, **364**, 1105
- Tegmark M., et al., 2004, *Phys. Rev. D*, **69**, 103501
- Tempel E., Stoica R. S., Saar E., 2013, *MNRAS*, **428**, 1827
- Tempel E., Libeskind N. I., Hoffman Y., Liivamägi L. J., Tamm A., 2014a, *MNRAS*, **437**, L11
- Tempel E., Stoica R. S., Martínez V. J., Liivamägi L. J., Castellan G., Saar E., 2014b, *MNRAS*, **438**, 3465
- Tully R. B., Shaya E. J., Karachentsev I. D., Courtois H. M., Kocevski D. D., Rizzi L., Peel A., 2008, *ApJ*, **676**, 184
- Tully R. B., Courtois H. M., Sorce J. G., 2016, *AJ*, **152**, 50
- Wang X., Szalay A., Aragón-Calvo M. A., Neyrinck M. C., Eyink G. L., 2014, *ApJ*, **793**, 58
- Welker C., et al., 2020, *MNRAS*, **491**, 2864
- White S. D. M., 1984, *ApJ*, **286**, 38
- White S. D. M., Frenk C. S., Davis M., Efstathiou G., 1987, *ApJ*, **313**, 505
- Wilde M. C., Elek O., Burchett J. N., Nagai D., Prochaska J. X., Werk J., Tuttle S., Forbes A. G., 2023, [arXiv e-prints](https://arxiv.org/abs/2301.02719), p. [arXiv:2301.02719](https://arxiv.org/abs/2301.02719)
- Wilding G., 2022, PhD thesis, University of Groningen, doi:10.33612/diss.250010290
- Wilding G., Nevenzeel K., van de Weygaert R., Vegter G., Pranav P., Jones B. J. T., Efstathiou K., Feldbrugge J., 2021, *MNRAS*, **507**, 2968
- Zeldovich Y. B., 1970, *A&A*, **500**, 13
- Zhang B., Lee K.-G., Krolewski A., Shi J., Horowitz B., Kooistra R., 2023, *ApJ*, **954**, 49
- de Graaff A., Cai Y.-C., Heymans C., Peacock J. A., 2019, *A&A*, **624**, A48
- de Lapparent V., Geller M. J., Huchra J. P., 1986, *ApJ*, **302**, L1
- de la Torre S., et al., 2013, *A&A*, **557**, A54
- van de Weygaert R., 2016, Voids and the Cosmic Web: cosmic depression & spatial complexity. pp 493–523 ([arXiv:1611.01222](https://arxiv.org/abs/1611.01222)), doi:10.1017/S1743921316010504
- van de Weygaert R., Babul A., 1994, *ApJ*, **425**, L59
- van de Weygaert R., Bernardeau F., 1998, in Proceedings of the 12th Potsdam Cosmology Workshop. pp 207–216 ([arXiv:astro-ph/9803143](https://arxiv.org/abs/astro-ph/9803143)), doi:10.48550/arXiv.astro-ph/9803143
- van de Weygaert R., Bond J. R., 2008a, Clusters and the Theory of the Cosmic Web. p. 335, doi:10.1007/978-1-4020-6941-3_10
- van de Weygaert R., Bond J. R., 2008b, Clusters and the Theory of the Cosmic Web. p. 335, doi:10.1007/978-1-4020-6941-3_10
- van de Weygaert R., Platen E., 2011, in International Journal of Modern Physics Conference Series. pp 41–66 ([arXiv:0912.2997](https://arxiv.org/abs/0912.2997)), doi:10.1142/S2010194511000092
- van de Weygaert R., Schaap W., 2009, in Martínez V. J., Saar E., Martínez-González E., Pons-Bordería M. J., eds, , Vol. 665, Data Analysis in Cosmology. pp 291–413, doi:10.1007/978-3-540-44767-2_11
- van de Weygaert R., van Kampen E., 1993, *MNRAS*, **263**, 481
- van de Weygaert R., Shandarin S., Saar E., Einasto J., eds, 2014, Proceedings, IAU Symposium 308: The Zeldovich Universe: Genesis and Growth of the Cosmic Web: Tallinn, Estonia, June 23-28, 2014

APPENDIX A: MMF/NEXUS & COSMIC WEB CLASSIFICATION

The NEXUS suite of cosmic web identifiers represents an elaboration and extension of the original Multiscale Morphology Filter (Aragón-Calvo et al. 2007b, 2010) algorithm and was developed with the goal of obtaining a more physically motivated and robust method. NEXUS+ is the principal representative of the full NEXUS suite of cosmic web identifiers (see Cautun et al. 2013). These include the options for multiscale morphology identifiers on the basis of the linear density, the logarithmic density, the velocity divergence, the velocity shear and tidal force field. NEXUS has incorporated these options in a versatile code for the analysis of cosmic web structure and dynamics following the realisation that they are significant physical influences

in shaping the cosmic mass distribution into the complexity of the cosmic web.

A1 Hessian Geometry and Morphological Identity

The basic setup of MMF/Nexus is that of defining a four-dimensional scale-space representation of the input field $f(\vec{x})$. In nearly all implementations this is achieved by means of a Gaussian filtering of $f(\vec{x})$ over a set of scales $[R_0, R_1, \dots, R_N]$,

$$f_{R_n}(\vec{x}) = \int \frac{d^3k}{(2\pi)^3} e^{-k^2 R_n^2/2} \hat{f}(\vec{k}) e^{i\vec{k}\cdot\vec{x}}, \quad (\text{A1})$$

where $\hat{f}(\vec{k})$ is the Fourier transform of the input field $f(\vec{x})$. The Hessian $H_{ij,R_n}(\vec{x})$ of the filtered field on the scale R_n is computed in Fourier space on the basis of the corresponding Fourier components $\hat{H}_{ij,R_n}(\vec{k})$,

$$H_{ij,R_n}(\vec{x}) = R_n^2 \frac{\partial^2 f_{R_n}(\vec{x})}{\partial x_i \partial x_j}. \quad (\text{A2})$$

$$\hat{H}_{ij,R_n}(\vec{k}) = -k_i k_j R_n^2 \hat{f}(\vec{k}) e^{-k^2 R_n^2/2}.$$

Note that the definition for the Hessian includes the normalisation term R_n^2 . The key element of the MMF/Nexus formalism is the morphological information contained in the eigenvalues of the Hessian matrix, $h_1 \leq h_2 \leq h_3$. By applying a set of morphology filters on these scaled eigenvalues (see Aragón-Calvo et al. 2007a; Cautun et al. 2013) this is translated into a scale dependent environment signature $S_{R_n}(\mathbf{x})$ that represents the geometry at the corresponding scale.

A2 Scale Space and Multiscale Structure

To analyse the multiscale nature of the cosmic web, the *Scale-Space* representation of the cosmic mass distributions produces a sequence of copies of the data having different resolutions (Florack et al. 1992; Lindeberg 1994). At each location \vec{x} in the probed volume, it involves an extra dimension, scale, that yields the eigenvalues of the Hessian filtered at the corresponding (Gaussian) scale and the scale dependent environment signature $S_{R_n}(\mathbf{x})$.

A feature searching algorithm is applied to the combined set of scaled copies in order to identify the scale at which, locally, we find the strongest morphological signature. It involves the combination of the complete set of scale-dependent environmental signatures to find the maximum signature for all scales

$$S(\mathbf{x}) = \max_{\text{levels } n} S_{R_n}(\mathbf{x}). \quad (\text{A3})$$

A3 Signature & Versions

The final step in the MMF/Nexus procedure involves the use of criteria to find the threshold signature that discriminates between valid and invalid morphological detections. Signature values larger than the threshold correspond to real structures while the rest are spurious detections. Different implementations and versions of the MMF/Nexus technique may differ in the definition of the threshold values.

The final outcome of the MMF/Nexus procedure is a field which at each location \vec{x} specifies what the local morphological signature is, cluster node, filaments, wall or void. The resulting field $\delta_j^{\text{NEXUS}}(\mathbf{x})$ is zero when the volume is not identified as cosmic web element j and is one when the volume elements is identified as element j . Here j is either filaments, nodes or walls. In this identification we also

intrinsically include the identification for voids which is defined as the volume elements that are neither a filament, node or wall.

Following the basic version of the MMF technique introduced by Aragón-Calvo et al. (2007a) it was applied to the analysis of the cosmic web in simulations of cosmic structure formation (Aragón-Calvo et al. 2010) and for finding filaments and galaxy-filament alignments in the SDSS galaxy distribution (Jones et al. 2010). The principal technique, and corresponding philosophy, has subsequently been branched in several further elaborations and developments Cautun et al. (2014); Aragón-Calvo & Yang (2014). Nexus (Cautun et al. 2014) has extended the MMF formalism to a substantially wider range of physical agents involved in the formation of the cosmic web, along with a substantially firmer foundation for the criteria used in identifying the various web-like structures. MMF-2 (Aragón-Calvo & Yang 2014) focuses with even more attention than the basic MMF formalism on the hierarchical nature of the cosmic web, by introducing and exploiting the concept of *hierarchical space*.

The NEXUS suite of cosmic web identifiers represents an elaboration and extension of the original Multiscale Morphology Filter (Aragón-Calvo et al. 2007b, 2010) algorithm and was developed with the goal of obtaining a more physically motivated and robust method. NEXUS+ is the principal representative of the full NEXUS suite of cosmic web identifiers (see Cautun et al. 2013). These include the options for multiscale morphology identifiers on the basis of the linear density, the logarithmic density, the velocity divergence, the velocity shear and tidal force field. NEXUS has incorporated these options in a versatile code for the analysis of cosmic web structure and dynamics following the realisation that they are significant physical influences in shaping the cosmic mass distribution into the complexity of the cosmic web.

A4 NEXUS+

NEXUS+ is the density field NEXUS version with the highest dynamic range. As input it takes a regularly sampled density field. In a first step, the input field is Gaussian smoothed using a LOGFILTER filter that is applied over a set of scales $[R_0, R_1, \dots, R_N]$, with $R_n = 2^{n/2} R_0$. It produces the logarithmic density field

$$\delta_+ = \log(1 + \delta(\mathbf{x})), \quad (\text{A4})$$

The logarithmic density field of NEXUS+ is better equipped to take account of the wide dynamic range of the nonlinear hierarchically evolved density field. The nonlinear field is highly non-Gaussian, with a large part of the volume having low-density values in combination with long high-density tails in the high-density cluster and filament regions. It translates into a nonlinear density field pdf that approaches a lognormal or skewed lognormal function.

For each of the included scale-space scales, NEXUS+ computes the eigenvalues of the Hessian matrix of the smoothed logarithmic density field. Using the Hessian eigenvalues of these, NEXUS+ computes an environmental signature for each volume element that characterises how close this region is to an ideal knot, filament and wall. Then, for each point, the environmental signatures computed for each scale are combined to obtain a scale independent signature.

In the last step, physical criteria are used to determine a detection threshold. All points with signature values above the threshold are valid structures. For knots, the threshold is given by the requirement that most knot-regions should be virialized. For filaments and walls, the threshold is determined on the basis of the change in filament and wall mass as a function of signature. The peak of the mass variation with signature delineates the most prominent filamentary and wall features of the cosmic web.

The NEXUS+ algorithm performs the environment detection by applying the above steps first to knots, then to filaments and finally to walls. Each volume element is assigned a single environment characteristic by requiring that filament regions cannot be knots and that walls regions cannot be either knots or filaments. The remaining regions are classified as voids.

This paper has been typeset from a \TeX/L\AA\TeX file prepared by the author.